Symplectic Contact Analysis of a Horizontally Laminated Magneto-electro-elastic Finite Specimen

Lizichen Chen[a], Weiqiu Chen[a,b,c,*]

[a]*Key Laboratory of Soft Machines and Smart Devices of Zhejiang Province, Department of Engineering Mechanics, Soft Matter Research Center, Zhejiang University, Hangzhou 310027, P.R. China*

[b]*Center for Soft Machines and Smart Devices, Huanjiang Laboratory, Zhuji 311816, P.R. China*

[c]*Faculty of Mechanical Engineering and Mechanics, Ningbo University, Ningbo 315211, P.R. China*

Abstract

This work formulates a symplectic framework for contact analysis of a horizontally laminated, magneto-electro-elastic, finite specimen. By incorporating dual variables and deriving the Hamiltonian operator matrix within the symplectic space, the constraints on the state variables are fulfilled through the property of symplectic orthogonality. The state variables between different layers are connected via the transfer matrices, and the Hamiltonian mixed energy variational principle is generalized for the laminated medium. Distinct from traditional methods, the symplectic framework offers a more realistic and efficient analysis approach for a finite-sized specimen, applicable to indenters with arbitrary profiles but predetermined contact region. The interfacial and boundary effects are explored, with remarkably accurate results as compared to the finite element simulations. This research not only enhances our understanding of the underlying phenomena but also lays a foundation for materials characterization using high-throughput testing techniques.

Keywords: Symplectic framework; Contact analysis; Horizontally laminated specimen; Interfacial and boundary effects

---

* *Corresponding author*. Tel./Fax: 85-571-87951866; *E-mail*: chenwq@zju.edu.cn (Weiqiu Chen).

This paper has been accepted by *Mechanics of Advanced Materials and Structures*

1. Introduction

Heterogeneous materials, characterized by the inherent non-uniformity in composition, structure, and properties, have garnered significant attention in recent years due to their pivotal role in advancing material science and engineering (Shen, 2010; Uchida et al., 2024). The heterogeneity-induced complexity necessitates the development of advanced characterization techniques that can capture and analyze the variations of material properties efficiently (Robertson et al., 2011; Jagadeesh et al., 2024).

High-throughput characterization (HTC) of heterogeneous materials, on the other hand, has emerged as a transformative approach, enabling rapid screening and assessment of material properties at an unprecedented scale (Wodo et al., 2015; Lu et al., 2024). This technology leverages a suite of rapid and multi-scale analytical methods to systematically probe the composition, structure, and various performance metrics of materials, thereby accelerating the discovery and optimization of novel materials. The concept of HTC takes root in the Materials Genome Initiative, which aims to streamline the materials development process by integrating high-throughput experiments, computation, and data analytics (Xu et al., 2023). By leveraging advanced technologies such as synchrotron radiation source and spallation neutron source, researchers can now obtain comprehensive datasets encompassing the composition, structure, and various performance parameters of materials (Wu et al., 2021). Among numerous approaches to material characterization, contact-based techniques have always been a crucial tool, witnessing widespread adoption recently for the assessment of inhomogeneous materials (Swaddiwudhipong et al., 2005). However, heterogeneous-specimen-based HTC techniques, in

general, still rely on the classical Hertzian contact theory (Hertz, 1881) to deduce material properties from experimental results. The effect of material inhomogeneity on contact responses therefore has been totally ignored in practical material characterization.

Theoretical contact analysis of heterogeneous materials is very difficult (Giannakopoulos and Suresh, 1997a, 1997b). Itou and Shima (1999) pioneered the use of a laminated model, in which each layer is assumed to be uniform. Ke and Wang (2006, 2007) further refined the model by assuming a linear distribution of material constant in every layer so that it can better approximate arbitrary variations of material properties. Notably, the layering direction of almost all contact models is along the depth (width in this paper), while that along the horizontal direction remains unexplored. Additionally, the existing models often adopt half-plane/half-space assumptions, which inadequately capture the physical reality that a specimen is usually of finite size. That is to say, these models also neglect the boundary effects (Stan and King, 2020). Hence, it is necessary to develop an effective method to overcome the difficulties inherent to the horizontally laminated contact model.

This work establishes the two-dimensional symplectic contact framework for a rigid punch with arbitrary profile acting over a determined region of a horizontally laminated magneto-electro-elastic finite specimen. The governing equations and symplectic orthogonality are presented in Section 2.1, and the corresponding eigen-solutions for zero and general eigenvalues are derived analytically in Sections 2.2 and 2.3, respectively, both contributing to the complete solutions in the symplectic expansion in Section 2.4. The interfacial and boundary effects are discussed in Section 3, where finite element simulations are performed for verification. Concluding remarks are illustrated in Section 4.

2. Contact analysis of a horizontally laminated magneto-electro-elastic finite specimen

We commence by considering a rigid punch of an arbitrary profile applied on the surface of a horizontally laminated, magneto-electro-elastic (MEE), finite specimen with the poling direction along the z-axis, as depicted in Fig. 1. The contact region is given to be $x \in [\tilde{a}, \tilde{b}]$. We consider a two-dimensional (plane-strain) model, and the specimen occupies the region of width h and length l. The poled MEE material is transversely isotropic, with $c_{ij}, e_{ij}, q_{ij}, \varepsilon_{ij}, \gamma_{ij}$, and d_{ij} being the elastic, piezoelectric, piezomagnetic, dielectric, magnetic and electromagnetic constants, respectively. All these are constant in every layer but are generally distinct in different layers. To be clear, we denote them in the k-th layer as $c_{ij;k}, e_{ij;k}, q_{ij;k}, \varepsilon_{ij;k}, \gamma_{ij;k}$, and $d_{ij;k}$, respectively. The thickness of the k-th layer is set to be $x_k - x_{k-1} \quad (k = 1, \cdots, n)$, and we have $x_n = l$.

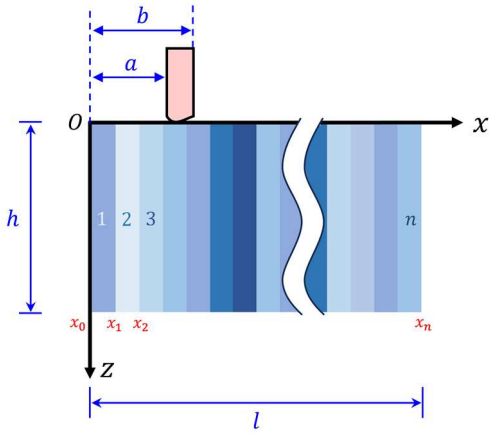

Fig. 1. A rigid punch acts on the surface of a horizontally laminated magneto-electro-elastic finite specimen of width h and length l.

2.1. Derivation of eigen equation

Under the plane-strain state assumption, the two-dimensional constitutive relations for the k-th layer are in the form of:

$$\begin{cases} \sigma_{xx;k} = c_{11;k}\dfrac{\partial u_{x;k}}{\partial x} + c_{13;k}\dfrac{\partial u_{z;k}}{\partial z} + e_{31;k}\dfrac{\partial \varphi_k}{\partial z} + q_{31;k}\dfrac{\partial \psi_k}{\partial z} \\ \sigma_{zz;k} = c_{13;k}\dfrac{\partial u_{x;k}}{\partial x} + c_{33;k}\dfrac{\partial u_{z;k}}{\partial z} + e_{33;k}\dfrac{\partial \varphi_k}{\partial z} + q_{33;k}\dfrac{\partial \psi_k}{\partial z} \\ \sigma_{xz;k} = c_{44;k}\left(\dfrac{\partial u_{x;k}}{\partial z} + \dfrac{\partial u_{z;k}}{\partial x}\right) + e_{15;k}\dfrac{\partial \varphi_k}{\partial x} + q_{15;k}\dfrac{\partial \psi_k}{\partial x} \\ D_{x;k} = e_{15;k}\left(\dfrac{\partial u_{x;k}}{\partial z} + \dfrac{\partial u_{z;k}}{\partial x}\right) - \varepsilon_{11;k}\dfrac{\partial \varphi_k}{\partial x} - d_{11;k}\dfrac{\partial \psi_k}{\partial x} \\ D_{z;k} = e_{31;k}\dfrac{\partial u_{x;k}}{\partial x} + e_{33;k}\dfrac{\partial u_{z;k}}{\partial z} - \varepsilon_{33;k}\dfrac{\partial \varphi_k}{\partial z} - d_{33;k}\dfrac{\partial \psi_k}{\partial z} \\ B_{x;k} = q_{15;k}\left(\dfrac{\partial u_{x;k}}{\partial z} + \dfrac{\partial u_{z;k}}{\partial x}\right) - d_{11;k}\dfrac{\partial \varphi_k}{\partial x} - \gamma_{11;k}\dfrac{\partial \psi_k}{\partial x} \\ B_{z;k} = q_{31;k}\dfrac{\partial u_{x;k}}{\partial x} + q_{33;k}\dfrac{\partial u_{z;k}}{\partial z} - d_{33;k}\dfrac{\partial \varphi_k}{\partial z} - \gamma_{33;k}\dfrac{\partial \psi_k}{\partial z} \end{cases} \tag{1}$$

where $\sigma_{ij;k}$ are the stress components; $u_{x;k}$ and $u_{z;k}$ are the displacement components in the x- and z-directions, respectively; φ_k and ψ_k are the electric potential and magnetic potential, respectively; $D_{i;k}$ and $B_{i;k}$ are the components of the electric displacement and the magnetic induction, respectively. For the case of plane-stress, the material constants in Eq. (1) will change and take different values.

Zhong (1995) ingeniously introduced the symplectic system into elasticity, forming a new branch called symplectic elasticity. This new approach was initially applied to investigate beams and plates with homogeneous and vertically layered materials (Yao et al., 2009), which has demonstrated its versatility and potential to tackle even more complex material behaviors. Chen and Chen (2024) recently proposed a symplectic approach to contact of an exponentially graded material. In this work, we will develop a significantly different symplectic framework for contact analysis of heterogeneous materials, which necessitates the fulfillment of continuity conditions

at the interfaces. To do so, we derive the following state equations from Eq. (1), together with the equilibrium equations without body forces:

$$\begin{cases} \dfrac{\partial u_{x;k}}{\partial z} = -\dfrac{\partial u_{z;k}}{\partial x} - a_{1;k}\dfrac{\partial \varphi_k}{\partial x} - a_{2;k}\dfrac{\partial \psi_k}{\partial x} + a_{3;k}\sigma_{xz;k} \\ \dfrac{\partial u_{z;k}}{\partial z} = -a_{4;k}\dfrac{\partial u_{x;k}}{\partial x} + a_{5;k}\sigma_{zz;k} + a_{6;k}D_{z;k} + a_{7;k}B_{z;k} \\ \dfrac{\partial \varphi_k}{\partial z} = a_{8;k}\dfrac{\partial u_{x;k}}{\partial x} + a_{6;k}\sigma_{zz;k} - a_{9;k}D_{z;k} + a_{10;k}B_{z;k} \\ \dfrac{\partial \psi_k}{\partial z} = a_{11;k}\dfrac{\partial u_{x;k}}{\partial x} + a_{7;k}\sigma_{zz;k} + a_{10;k}D_{z;k} - a_{12;k}B_{z;k} \\ \dfrac{\partial \sigma_{xz;k}}{\partial z} = a_{13;k}\dfrac{\partial^2 u_{x;k}}{\partial x^2} - a_{4;k}\dfrac{\partial \sigma_{zz;k}}{\partial x} + a_{8;k}\dfrac{\partial D_{z;k}}{\partial x} + a_{11;k}\dfrac{\partial B_{z;k}}{\partial x} \\ \dfrac{\partial \sigma_{zz;k}}{\partial z} = -\dfrac{\partial \sigma_{xz;k}}{\partial x} \\ \dfrac{\partial D_{z;k}}{\partial z} = a_{14;k}\dfrac{\partial^2 \varphi_k}{\partial x^2} + a_{15;k}\dfrac{\partial^2 \psi_k}{\partial x^2} - a_{1;k}\dfrac{\partial \sigma_{xz;k}}{\partial x} \\ \dfrac{\partial B_{z;k}}{\partial z} = a_{15;k}\dfrac{\partial^2 \varphi_k}{\partial x^2} + a_{16;k}\dfrac{\partial^2 \psi_k}{\partial x^2} - a_{2;k}\dfrac{\partial \sigma_{xz;k}}{\partial x} \end{cases} \tag{2}$$

and the supplementary equations as

$$\begin{cases} \sigma_{xx;k} = -a_{13;k}\dfrac{\partial u_{x;k}}{\partial x} + a_{4;k}\sigma_{zz;k} - a_{8;k}D_{z;k} - a_{11;k}B_{z;k} \\ D_{x;k} = -a_{14;k}\dfrac{\partial \varphi_k}{\partial x} - a_{15;k}\dfrac{\partial \psi_k}{\partial x} + a_{1;k}\sigma_{xz;k} \\ B_{x;k} = -a_{15;k}\dfrac{\partial \varphi_k}{\partial x} - a_{16;k}\dfrac{\partial \psi_k}{\partial x} + a_{2;k}\sigma_{xz;k} \end{cases} \tag{3}$$

where $a_{i;k}$ in Eqs. (2) and (3) are material-constants-related coefficients, which are tabulated in Appendix A. By introducing the state vector $\boldsymbol{f}$ in the k-th layer

$$\boldsymbol{f}_k = [\boldsymbol{q}_k, \boldsymbol{p}_k]^{\mathrm{T}} = \left[[u_{x;k}, u_{z;k}, \varphi_k, \psi_k], [\sigma_{xz;k}, \sigma_{zz;k}, D_{z;k}, B_{z;k}]\right]^{\mathrm{T}} \tag{4}$$

where the components in $\boldsymbol{q}_k$ and $\boldsymbol{p}_k$ are dual variables. Eq. (2) may be rewritten in canonical matrix form as

$$\frac{\partial}{\partial z}\mathbf{I}_8 \boldsymbol{f}_k = \boldsymbol{\mathcal{H}}_k \boldsymbol{f}_k \tag{5}$$

where $\mathbf{I}_n$ is the nth-order identity matrix, and $\boldsymbol{\mathcal{H}}_k$ is the operator matrix given by

$$\boldsymbol{\mathcal{H}}_k=\left[\begin{array}{cccc|cccc}
0 & -\dfrac{\partial}{\partial x} & -a_{1;k}\dfrac{\partial}{\partial x} & -a_{2;k}\dfrac{\partial}{\partial x} & a_{3;k} & 0 & 0 & 0 \\
-a_{4;k}\dfrac{\partial}{\partial x} & 0 & 0 & 0 & 0 & a_{5;k} & a_{6;k} & a_{7;k} \\
a_{8;k}\dfrac{\partial}{\partial x} & 0 & 0 & 0 & 0 & a_{6;k} & -a_{9;k} & a_{10;k} \\
a_{11;k}\dfrac{\partial}{\partial x} & 0 & 0 & 0 & 0 & a_{7;k} & a_{10;k} & -a_{12;k} \\
\hline
a_{13;k}\dfrac{\partial^2}{\partial x^2} & 0 & 0 & 0 & 0 & -a_{4;k}\dfrac{\partial}{\partial x} & a_{8;k}\dfrac{\partial}{\partial x} & a_{11;k}\dfrac{\partial}{\partial x} \\
0 & 0 & 0 & 0 & -\dfrac{\partial}{\partial x} & 0 & 0 & 0 \\
0 & 0 & a_{14;k}\dfrac{\partial^2}{\partial x^2} & a_{15;k}\dfrac{\partial^2}{\partial x^2} & -a_{1;k}\dfrac{\partial}{\partial x} & 0 & 0 & 0 \\
0 & 0 & a_{15;k}\dfrac{\partial^2}{\partial x^2} & a_{16;k}\dfrac{\partial^2}{\partial x^2} & -a_{2;k}\dfrac{\partial}{\partial x} & 0 & 0 & 0
\end{array}\right] \tag{6}$$

We subsequently introduce the unit symplectic matrix, which functions as a basis in establishing the symplectic orthogonality with respect to the operator matrix $\boldsymbol{\mathcal{H}}_k$, as

$$\mathbf{J}=\begin{bmatrix} 0 & \mathbf{I}_4 \\ -\mathbf{I}_4 & 0 \end{bmatrix} \tag{7}$$

and denote the symplectic inner product as

$$\begin{aligned}
\left\langle \boldsymbol{f}^{\alpha},\boldsymbol{f}^{\beta}\right\rangle &= \sum_{k=1}^{n}\int_{x_{k-1}}^{x_k}\left(\boldsymbol{f}_k^{\alpha}\right)^{\mathrm{T}}\mathbf{J}\boldsymbol{f}_k^{\beta}\mathrm{d}x \\
&= \sum_{k=1}^{n}\int_{x_{k-1}}^{x_k}(u_{x;k}^{\alpha}\sigma_{xz;k}^{\beta}+u_{z;k}^{\alpha}\sigma_{zz;k}^{\beta}+\varphi_k^{\alpha}D_{z;k}^{\beta}+\psi_k^{\alpha}B_{z;k}^{\beta} \\
&\quad -\sigma_{xz;k}^{\alpha}u_{x;k}^{\beta}-\sigma_{zz;k}^{\alpha}u_{z;k}^{\beta}-D_{z;k}^{\alpha}\varphi_k^{\beta}-B_{z;k}^{\alpha}\psi_k^{\beta})\mathrm{d}x
\end{aligned} \tag{8}$$

Here, $\boldsymbol{f}\triangleq\bigcup_{k=1}^{n}\boldsymbol{f}_k$ is a piecewise continuous global vector function formed by $\boldsymbol{f}_k$ $(k=1,2,\cdots,n)$ in the x-direction, and the superscript α or β denotes a specified global vector. In the following, the subscript k will be omitted for brevity, unless it is necessary to avoid any potential confusion.

The symplectic inner product defined in Eq. (8) has the following properties (Yao et al., 2009):

$$\begin{aligned}
&\left\langle \boldsymbol{f}^{\alpha},\boldsymbol{f}^{\beta}\right\rangle=-\left\langle \boldsymbol{f}^{\beta},\boldsymbol{f}^{\alpha}\right\rangle \\
&\left\langle c\boldsymbol{f}^{\alpha},\boldsymbol{f}^{\beta}\right\rangle=c\left\langle \boldsymbol{f}^{\alpha},\boldsymbol{f}^{\beta}\right\rangle, \qquad c\in\mathbb{R} \\
&\left\langle \boldsymbol{f}^{\alpha}+\boldsymbol{f}^{\gamma},\boldsymbol{f}^{\beta}\right\rangle=\left\langle \boldsymbol{f}^{\alpha},\boldsymbol{f}^{\beta}\right\rangle+\left\langle \boldsymbol{f}^{\gamma},\boldsymbol{f}^{\beta}\right\rangle, \qquad \boldsymbol{f}^{\alpha},\boldsymbol{f}^{\beta},\boldsymbol{f}^{\gamma}\in\mathscr{L} \\
&\boldsymbol{f}^{\alpha}=0,\ \text{if}\ \left\langle \boldsymbol{f}^{\alpha},\boldsymbol{f}^{\beta}\right\rangle=0\ \text{for every}\ \boldsymbol{f}^{\beta}\in\mathscr{L}
\end{aligned} \tag{9}$$

where $\mathscr{L}$ is a linear space defined in $\mathbb{R}$. The global state vectors satisfying Eq. (9) construct a symplectic space. Utilizing the technique of integration by parts, along with the homogeneous

boundary conditions at the lateral boundaries

$$x=x_0:\begin{cases}-a_{13;1}\dfrac{\partial u_{x;1}}{\partial x}+a_{4;1}\sigma_{zz;1}-a_{8;1}D_{z;1}-a_{11;1}B_{z;1}=0\\ \sigma_{xz;1}=0\\ -a_{14;1}\dfrac{\partial \varphi_1}{\partial x}-a_{15;1}\dfrac{\partial \psi_1}{\partial x}+a_{1;1}\sigma_{xz;1}=0\\ -a_{15;1}\dfrac{\partial \varphi_1}{\partial x}-a_{16;1}\dfrac{\partial \psi_1}{\partial x}+a_{2;1}\sigma_{xz;1}=0\end{cases} \tag{10}$$

$$x=x_n:\begin{cases}-a_{13;n}\dfrac{\partial u_{x;n}}{\partial x}+a_{4;n}\sigma_{zz;n}-a_{8;n}D_{z;n}-a_{11;n}B_{z;n}=0\\ \sigma_{xz;n}=0\\ -a_{14;n}\dfrac{\partial \varphi_n}{\partial x}-a_{15;n}\dfrac{\partial \psi_n}{\partial x}+a_{1;n}\sigma_{xz;n}=0\\ -a_{15;n}\dfrac{\partial \varphi_n}{\partial x}-a_{16;n}\dfrac{\partial \psi_n}{\partial x}+a_{2;n}\sigma_{xz;n}=0\end{cases} \tag{11}$$

and the continuity conditions at the interfaces,

$$\begin{cases}u_{x;k}(x_k)=u_{x;k+1}(x_k), & \sigma_{xx;k}(x_k)=\sigma_{xx;k+1}(x_k)\\ u_{z;k}(x_k)=u_{z;k+1}(x_k), & \sigma_{xz;k}(x_k)=\sigma_{xz;k+1}(x_k)\\ \varphi_k(x_k)=\varphi_{k+1}(x_k), & D_{x;k}(x_k)=D_{x;k+1}(x_k)\\ \psi_k(x_k)=\psi_{k+1}(x_k), & B_{x;k}(x_k)=B_{x;k+1}(x_k)\end{cases} \tag{12}$$

we can prove that

$$\left\langle \boldsymbol{f}^{\alpha},\boldsymbol{\mathcal{H}}\boldsymbol{f}^{\beta}\right\rangle=\left\langle \boldsymbol{f}^{\beta},\boldsymbol{\mathcal{H}}\boldsymbol{f}^{\alpha}\right\rangle \tag{13}$$

Hence, $\boldsymbol{\mathcal{H}}\triangleq\bigcup_{k=1}^{n}\boldsymbol{\mathcal{H}}_k$ is the global Hamiltonian operator matrix, the eigenvectors of which are mutually adjoint symplectic-orthogonal.

Generally, we postulate that the solution can be expressed as

$$\boldsymbol{f}_k(x,z)=\boldsymbol{\Phi}_k(x)\xi(z)=[u_k(x),w_k(x),\phi_k(x),\psi_k(x),\tau_k(x),\sigma_k(x),D_k(x),B_k(x)]^{\mathrm{T}}\xi(z) \tag{14}$$

Substituting Eq. (14) into Eq. (5) for separation of variables yields

$$\frac{\dfrac{\partial}{\partial z}\xi(z)}{\xi(z)}=\left[\boldsymbol{\mathcal{H}}_k\boldsymbol{\Phi}_k(x)\right]\boldsymbol{\Phi}_k^{-1}(x) \tag{15}$$

which leads to

$$\xi(z)=\mathrm{e}^{\mu z} \tag{16}$$

along with the eigen equation

$$\boldsymbol{\mathcal{H}}_k \boldsymbol{\Phi}_k(x) = \mu \boldsymbol{\Phi}_k(x) \tag{17}$$

where μ is the eigenvalue, and $\boldsymbol{\Phi}_k(x)$ is the eigenvector. It is noted that all the layers share the same set of μ (together with $\xi(z)$), since the continuity conditions should be satisfied at the interfaces, as elucidated in Section 2.3.

2.2. Eigen-solutions for zero eigenvalue

The zero eigenvalue is a special eigenvalue, since the displacement and stress components of the corresponding solutions don't exponentially decay in the z-direction. The corresponding state equations are

$$\begin{cases} -\dfrac{\partial w_k}{\partial x} - a_{1;k}\dfrac{\partial \phi_k}{\partial x} - a_{2;k}\dfrac{\partial \psi_k}{\partial x} + a_{3;k}\tau_k = 0 \\ -a_{4;k}\dfrac{\partial u_k}{\partial x} + a_{5;k}\sigma_k + a_{6;k}D_k + a_{7;k}B_k = 0 \\ a_{8;k}\dfrac{\partial u_k}{\partial x} + a_{6;k}\sigma_k - a_{9;k}D_k + a_{10;k}B_k = 0 \\ a_{11;k}\dfrac{\partial u_k}{\partial x} + a_{7;k}\sigma_k + a_{10;k}D_k - a_{12;k}B_k = 0 \\ a_{13;k}\dfrac{\partial^2 u_k}{\partial x^2} - a_{4;k}\dfrac{\partial \sigma_k}{\partial x} + a_{8;k}\dfrac{\partial D_k}{\partial x} + a_{11;k}\dfrac{\partial B_k}{\partial x} = 0 \\ -\dfrac{\partial \tau_k}{\partial x} = 0 \\ a_{14;k}\dfrac{\partial^2 \phi_k}{\partial x^2} + a_{15;k}\dfrac{\partial^2 \psi_k}{\partial x^2} - a_{1;k}\dfrac{\partial \tau_k}{\partial x} = 0 \\ a_{15;k}\dfrac{\partial^2 \phi_k}{\partial x^2} + a_{16;k}\dfrac{\partial^2 \psi_k}{\partial x^2} - a_{2;k}\dfrac{\partial \tau_k}{\partial x} = 0 \end{cases} \tag{18}$$

The eigenvectors of Eq. (18) satisfying the homogeneous boundary conditions and continuity conditions are

$$\begin{aligned} \boldsymbol{f}^{(0)}_{0,1;k} &= \boldsymbol{\Phi}^{(0)}_{0,1;k} = [1,0,0,0,0,0,0,0]^{\mathrm{T}}, \quad \boldsymbol{f}^{(0)}_{0,2;k} = \boldsymbol{\Phi}^{(0)}_{0,2;k} = [0,1,0,0,0,0,0,0]^{\mathrm{T}} \\ \boldsymbol{f}^{(0)}_{0,3;k} &= \boldsymbol{\Phi}^{(0)}_{0,3;k} = [0,0,1,0,0,0,0,0]^{\mathrm{T}}, \quad \boldsymbol{f}^{(0)}_{0,4;k} = \boldsymbol{\Phi}^{(0)}_{0,4;k} = [0,0,0,1,0,0,0,0]^{\mathrm{T}} \end{aligned} \tag{19}$$

where the superscript stands for the order of Jordan form, and the subscripts

$0,t;k$ $(t=1,\cdots,4;k=1,\cdots,n)$ represent the t-th Jordan chain for zero eigenvalue in the k-th layer. It is advisable to derive the eigenvectors of the first layer with the lateral boundary conditions at $x=x_0$, and then transfer the results via the continuity conditions layer by layer. In addition, the eigen-solutions remain the same as the eigenvectors in the zero-eigenvalue case, which are in accordance with the fact that exponential decay terms are absent.

The first-order Jordan form eigenvectors for zero eigenvalue are determined from

$$\boldsymbol{\mathcal{H}}_k\boldsymbol{\Phi}_{0,t;k}^{(1)}=\boldsymbol{\Phi}_{0,t;k}^{(0)}\quad(t=1,2,\cdots,4) \tag{20}$$

We then get

$$\begin{aligned}
\boldsymbol{\Phi}_{0,1;k}^{(1)}&=[0,-x+\theta_1,0,0,0,0,0,0]^{\mathrm{T}}\\
\boldsymbol{\Phi}_{0,2;k}^{(1)}&=[-a_{17;k}x+\tilde{\beta}_{1;k},0,0,0,0,\rho_{1;k},\rho_{2;k},\rho_{3;k}]^{\mathrm{T}}\\
\boldsymbol{\Phi}_{0,3;k}^{(1)}&=[-a_{18;k}x+\tilde{\beta}_{2;k},0,0,0,0,\rho_{4;k},\rho_{5;k},\rho_{6;k}]^{\mathrm{T}}\\
\boldsymbol{\Phi}_{0,4;k}^{(1)}&=[-a_{19;k}x+\tilde{\beta}_{3;k},0,0,0,0,\rho_{7;k},\rho_{8;k},\rho_{9;k}]^{\mathrm{T}}
\end{aligned} \tag{21}$$

where $\rho_{i;k}$ are constants, as detailed in Appendix A, and θ_1 is a coefficient determined via the symplectic orthogonality condition:

$$\begin{aligned}
\left\langle\boldsymbol{\Phi}_{0,2}^{(1)},\boldsymbol{\Phi}_{0,1}^{(1)}\right\rangle&=\sum_{k=1}^{n}\int_{x_{k-1}}^{x_k}\rho_{1;k}(x-\theta_1)\mathrm{d}x\\
&=\sum_{k=1}^{n}\frac{\rho_{1;k}}{2}(x_k^2-x_{k-1}^2)-\theta_1\sum_{k=1}^{n}\rho_{1;k}(x_k-x_{k-1})\\
&=0
\end{aligned} \tag{22}$$

which gives

$$\theta_1=\frac{\sum_{k=1}^{n}\frac{\rho_{1;k}}{2}(x_k^2-x_{k-1}^2)}{\sum_{k=1}^{n}\rho_{1;k}(x_k-x_{k-1})} \tag{23}$$

It is worth noting that θ_1 determined above fulfills the homogeneous lateral boundary condition $\tau_n=0$ at $x=x_n$, which is elaborated in Appendix B. $\tilde{\beta}_{i;k}$ are deduced according to the continuity conditions:

$$\begin{aligned}
&\tilde{\beta}_{1;(k+1)} = (a_{17;(k+1)} - a_{17;k})x_k + \tilde{\beta}_{1;k} \\
&\tilde{\beta}_{2;(k+1)} = (a_{18;(k+1)} - a_{18;k})x_k + \tilde{\beta}_{2;k} \quad (k = 1,2,\cdots,n-1) \\
&\tilde{\beta}_{3;(k+1)} = (a_{19;(k+1)} - a_{19;k})x_k + \tilde{\beta}_{3;k} \\
&\tilde{\beta}_{1;1} = 0, \quad \tilde{\beta}_{2;1} = 0, \quad \tilde{\beta}_{3;1} = 0
\end{aligned} \tag{24}$$

The first-order Jordan form eigenvectors in Eq. (21) no longer serve as solutions of Eq. (18). Instead, the desired eigen-solutions should be reformulated in a new manner:

$$\boldsymbol{f}_{0,t;k}^{(1)} = \boldsymbol{\Phi}_{0,t;k}^{(1)} + z\boldsymbol{\Phi}_{0,t;k}^{(0)} \quad (t = 1,2,\cdots,4) \tag{25}$$

Similarly, the second-order Jordan form eigenvectors should be determined from

$$\boldsymbol{\mathcal{H}}_k \boldsymbol{\Phi}_{0,t;k}^{(2)} = \boldsymbol{\Phi}_{0,t;k}^{(1)} \quad (t = 1,2,\cdots,4) \tag{26}$$

The last three equations in Eq. (26) (i.e., t = 2,3,4) do not lead to any eigenvector, making the chain of Jordan form eigen-solutions terminate. However, the eigenvector for the first equation of Eq. (26) can be obtained as

$$\boldsymbol{\Phi}_{0,1;k}^{(2)} = [\frac{a_{17;k}}{2}(x-\theta_1)^2 + \tilde{\beta}_{4;k}, 0, 0, 0, 0, -\rho_{1;k}(x-\theta_1), -\rho_{2;k}(x-\theta_1), -\rho_{3;k}(x-\theta_1)]^{\mathrm{T}} \tag{27}$$

where

$$\begin{aligned}
&\tilde{\beta}_{4;(k+1)} = \frac{a_{17;k} - a_{17;(k+1)}}{2}(x_k - \theta_1)^2 + \tilde{\beta}_{4;k} \quad (k = 1,2,\cdots,n-1) \\
&\tilde{\beta}_{4;1} = 0
\end{aligned} \tag{28}$$

The corresponding eigen-solution is given by

$$\boldsymbol{f}_{0,1;k}^{(2)} = \boldsymbol{\Phi}_{0,1;k}^{(2)} + z\boldsymbol{\Phi}_{0,1;k}^{(1)} + \frac{z^2}{2}\boldsymbol{\Phi}_{0,1;k}^{(0)} \tag{29}$$

The third-order Jordan form eigenvector satisfies

$$\boldsymbol{\mathcal{H}}_k \boldsymbol{\Phi}_{0,1;k}^{(3)} = \boldsymbol{\Phi}_{0,1;k}^{(2)} \tag{30}$$

from which we obtain

$$\boldsymbol{\Phi}_{0,1;k}^{(3)}=\begin{Bmatrix}0\\ -\frac{\rho_{15;k}}{6}(x-\theta_1)^3-\rho_{16;k}(x-\theta_1)+\tilde{\beta}_{10;k}\\ \frac{\rho_{11;k}}{6}(x-\theta_1)^3+\rho_{12;k}(x-\theta_1)+\tilde{\beta}_{8;k}\\ \frac{\rho_{13;k}}{6}(x-\theta_1)^3+\rho_{14;k}(x-\theta_1)+\tilde{\beta}_{9;k}\\ \frac{\rho_{1;k}}{2}(x-\theta_1)^2+\tilde{\beta}_{5;k}\\ 0\\ 0\\ 0\end{Bmatrix} \tag{31}$$

and the associated eigen-solution:

$$\boldsymbol{f}_{0,1;k}^{(3)}=\boldsymbol{\Phi}_{0,1;k}^{(3)}+z\boldsymbol{\Phi}_{0,1;k}^{(2)}+\frac{z^2}{2!}\boldsymbol{\Phi}_{0,1;k}^{(1)}+\frac{z^3}{3!}\boldsymbol{\Phi}_{0,1;k}^{(0)} \tag{32}$$

where

$$\begin{aligned}
&\tilde{\beta}_{5;(k+1)}=\frac{\rho_{1;k}-\rho_{1;(k+1)}}{2}(x_k-\theta_1)^2+\tilde{\beta}_{5;k}, && \tilde{\beta}_{5;1}=-\frac{\rho_{1;1}}{2}\theta_1^2\\
&\tilde{\beta}_{6;(k+1)}=\frac{\rho_{2;(k+1)}-\rho_{2;k}}{2}(x_k-\theta_1)^2+\tilde{\beta}_{6;k}, && \tilde{\beta}_{6;1}=\frac{\rho_{2;1}}{2}\theta_1^2\\
&\tilde{\beta}_{7;(k+1)}=\frac{\rho_{3;(k+1)}-\rho_{3;k}}{2}(x_k-\theta_1)^2+\tilde{\beta}_{7;k}, && \tilde{\beta}_{7;1}=\frac{\rho_{3;1}}{2}\theta_1^2\\
&\tilde{\beta}_{8;(k+1)}=\frac{\rho_{11;k}-\rho_{11;(k+1)}}{6}(x_k-\theta_1)^3+(\rho_{12;k}-\rho_{12;(k+1)})(x_k-\theta_1)+\tilde{\beta}_{8;k}, && \tilde{\beta}_{8;1}=0\\
&\tilde{\beta}_{9;(k+1)}=\frac{\rho_{13;k}-\rho_{13;(k+1)}}{6}(x_k-\theta_1)^3+(\rho_{14;k}-\rho_{14;(k+1)})(x_k-\theta_1)+\tilde{\beta}_{9;k}, && \tilde{\beta}_{9;1}=0\\
&\tilde{\beta}_{10;(k+1)}=\frac{\rho_{15;(k+1)}-\rho_{15;k}}{6}(x_k-\theta_1)^3+(\rho_{16;(k+1)}-\rho_{16;k})(x_k-\theta_1)+\tilde{\beta}_{10;k}, && \tilde{\beta}_{10;1}=0
\end{aligned} \qquad (k=1,2,\cdots,n-1)$$

It is noteworthy that no feasible solution satisfies the eigen equation corresponding to the fourth-order eigenvector, which indicates the Jordan chain terminates. Meanwhile, the correctness of $\boldsymbol{\Phi}_{0,1;k}^{(3)}$ may be verified by checking the state variable τ_n at $x=x_n$,

$$\begin{aligned}
\tau_n(x_n)&=\frac{\rho_{1;n}}{2}(x_n-\theta_1)^2+\tilde{\beta}_{5;n}\\
&=\frac{\rho_{1;n}}{2}(x_n-\theta_1)^2+\frac{\rho_{1;(n-1)}-\rho_{1;n}}{2}(x_{n-1}-\theta_1)^2+\tilde{\beta}_{5;(n-1)}\\
&=\frac{\rho_{1;n}}{2}[(x_n-\theta_1)^2-(x_{n-1}-\theta_1)^2]+\cdots+\frac{\rho_{1;1}}{2}[(x_1-\theta_1)^2-(x_0-\theta_1)^2]\\
&=\sum_{k=1}^{n}\frac{\rho_{1;k}}{2}(x_k^2-x_{k-1}^2)-\theta_1\sum_{k=1}^{n}\rho_{1;k}(x_k-x_{k-1})\\
&=0
\end{aligned} \tag{33}$$

which coincides with the homogeneous boundary conditions. Consequently, all the aforementioned eigenvectors form a symplectic subspace, which leads to the Saint-Venant solutions.

2.3. Eigen-solutions of general eigenvalues

The mixed boundary-value problems pertaining to contact and crack analyses are typically marked by the presence of sudden variations in external loads or prescribed displacements within certain domain. In the light of that, the general eigenvalues should be involved to fulfill the complex boundary conditions. The eigen equation is then constructed as

$$\begin{cases} -\dfrac{\partial w_k}{\partial x} - a_{1;k}\dfrac{\partial \phi_k}{\partial x} - a_{2;k}\dfrac{\partial \psi_k}{\partial x} + a_{3;k}\tau_k = \mu u_k \\ -a_{4;k}\dfrac{\partial u_k}{\partial x} + a_{5;k}\sigma_k + a_{6;k}D_k + a_{7;k}B_k = \mu w_k \\ a_{8;k}\dfrac{\partial u_k}{\partial x} + a_{6;k}\sigma_k - a_{9;k}D_k + a_{10;k}B_k = \mu \phi_k \\ a_{11;k}\dfrac{\partial u_k}{\partial x} + a_{7;k}\sigma_k + a_{10;k}D_k - a_{12;k}B_k = \mu \psi_k \\ a_{13;k}\dfrac{\partial^2 u_k}{\partial x^2} - a_{4;k}\dfrac{\partial \sigma_k}{\partial x} + a_{8;k}\dfrac{\partial D_k}{\partial x} + a_{11;k}\dfrac{\partial B_k}{\partial x} = \mu \tau_k \\ -\dfrac{\partial \tau_k}{\partial x} = \mu \sigma_k \\ a_{14;k}\dfrac{\partial^2 \phi_k}{\partial x^2} + a_{15;k}\dfrac{\partial^2 \psi_k}{\partial x^2} - a_{1;k}\dfrac{\partial \tau_k}{\partial x} = \mu D_k \\ a_{15;k}\dfrac{\partial^2 \phi_k}{\partial x^2} + a_{16;k}\dfrac{\partial^2 \psi_k}{\partial x^2} - a_{2;k}\dfrac{\partial \tau_k}{\partial x} = \mu B_k \end{cases} \tag{34}$$

where μ represents any nonzero eigenvalue. Supposing that the eigenvalue in the x-direction is η, and the determinant yields

$$\det\begin{bmatrix} -\mu & -\eta & -a_{1;k}\eta & -a_{2;k}\eta & a_{3;k} & 0 & 0 & 0 \\ -a_{4;k}\eta & -\mu & 0 & 0 & 0 & a_{5;k} & a_{6;k} & a_{7;k} \\ a_{8;k}\eta & 0 & -\mu & 0 & 0 & a_{6;k} & -a_{9;k} & a_{10;k} \\ a_{11;k}\eta & 0 & 0 & -\mu & 0 & a_{7;k} & a_{10;k} & -a_{12;k} \\ a_{13;k}\eta^2 & 0 & 0 & 0 & -\mu & -a_{4;k}\eta & a_{8;k}\eta & a_{11;k}\eta \\ 0 & 0 & 0 & 0 & -\eta & -\mu & 0 & 0 \\ 0 & 0 & a_{14;k}\eta^2 & a_{15;k}\eta^2 & -a_{1;k}\eta & 0 & -\mu & 0 \\ 0 & 0 & a_{15;k}\eta^2 & a_{16;k}\eta^2 & -a_{2;k}\eta & 0 & 0 & -\mu \end{bmatrix} = 0 \tag{35}$$

The above equation is further simplified as

$$\Lambda_{0;k}\left(\frac{\eta}{\mu}\right)^8 + \Lambda_{1;k}\left(\frac{\eta}{\mu}\right)^6 + \Lambda_{2;k}\left(\frac{\eta}{\mu}\right)^4 + \Lambda_{3;k}\left(\frac{\eta}{\mu}\right)^2 + 1 = 0 \tag{36}$$

where $\Lambda_{i;k}$ $(i=0,1,\cdots,3)$ are parameters that contain $a_{i;k}$, as given in Appendix C. The eight roots are derived analytically as

$$\eta_{1,2;k} = \pm\sqrt{\chi_{1;k}}\mu, \quad \eta_{3,4;k} = \pm\sqrt{\chi_{2;k}}\mu, \quad \eta_{5,6;k} = \pm\sqrt{\chi_{3;k}}\mu, \quad \eta_{7,8;k} = \pm\sqrt{\chi_{4;k}}\mu \tag{37}$$

where $\chi_{i;k}$ $(i=1,2,\cdots,4)$ can be found in Appendix C. Without loss of generality, the eigenvectors are established for the respective nonzero eigenvalues:

$$\boldsymbol{\Phi}_k = \sum_{t=1}^{8} \mathrm{e}^{\eta_{t;k}x}[\tilde{A}_{t;k}, \tilde{B}_{t;k}, \tilde{C}_{t;k}, \tilde{D}_{t;k}, \tilde{E}_{t;k}, \tilde{F}_{t;k}, \tilde{G}_{t;k}, \tilde{H}_{t;k}]^{\mathrm{T}} \tag{38}$$

where $\tilde{A}_{t;k}$, $\tilde{B}_{t;k}$, $\tilde{C}_{t;k}$, $\tilde{D}_{t;k}$, $\tilde{E}_{t;k}$, $\tilde{F}_{t;k}$, $\tilde{G}_{t;k}$, and $\tilde{H}_{t;k}$ are constants, the relations of which are obtained by substituting the eigenvectors into the eigen equation. It is noted that, if repeated roots exist, the eigenvectors will have different forms, as shown in Appendix C.

We then classify and represent the constants in terms of $\tilde{E}_{t;k}$:

$$\begin{aligned} \begin{Bmatrix} \tilde{A}_{t;k} \\ \tilde{B}_{t;k} \\ \tilde{C}_{t;k} \\ \tilde{D}_{t;k} \\ \tilde{F}_{t;k} \\ \tilde{G}_{t;k} \\ \tilde{H}_{t;k} \end{Bmatrix} &= \begin{bmatrix} -\mu & -\eta_{t;k} & -a_{1;k}\eta_{t;k} & -a_{2;k}\eta_{t;k} & 0 & 0 & 0 \\ -a_{4;k}\eta_{t;k} & -\mu & 0 & 0 & a_{5;k} & a_{6;k} & a_{7;k} \\ a_{8;k}\eta_{t;k} & 0 & -\mu & 0 & a_{6;k} & -a_{9;k} & a_{10;k} \\ a_{11;k}\eta_{t;k} & 0 & 0 & -\mu & a_{7;k} & a_{10;k} & -a_{12;k} \\ 0 & 0 & 0 & 0 & -\mu & 0 & 0 \\ 0 & 0 & a_{14;k}\eta_{t;k}^2 & a_{15;k}\eta_{t;k}^2 & 0 & -\mu & 0 \\ 0 & 0 & a_{15;k}\eta_{t;k}^2 & a_{16;k}\eta_{t;k}^2 & 0 & 0 & -\mu \end{bmatrix}^{-1} \begin{Bmatrix} -a_{3;k} \\ 0 \\ 0 \\ 0 \\ \eta_{t;k} \\ a_{1;k}\eta_{t;k} \\ a_{2;k}\eta_{t;k} \end{Bmatrix} \tilde{E}_{t;k} \\ &\equiv [\Upsilon_{1t;k}, \Upsilon_{2t;k}, \Upsilon_{3t;k}, \Upsilon_{4t;k}, \Upsilon_{5t;k}, \Upsilon_{6t;k}, \Upsilon_{7t;k}]^{\mathrm{T}} \tilde{E}_{t;k} \end{aligned} \tag{39}$$

where $\Upsilon_{jt;k}(j=1,\cdots,7;t=1,\cdots,8)$ are given in Appendix C. Next, $\tilde{A}_{t;k}$, $\tilde{B}_{t;k}$, $\tilde{C}_{t;k}$, $\tilde{D}_{t;k}$, $\tilde{F}_{t;k}$,

$\tilde{G}_{t;k}$, and $\tilde{H}_{t;k}$ in the homogeneous boundary conditions and continuity conditions are replaced with $\tilde{E}_{t;k}$:

$$\begin{cases} -a_{13;1}\dfrac{\partial u_1}{\partial x}+a_{4;1}\sigma_1-a_{8;1}D_1-a_{11;1}B_1\Big|_{x=x_0}=\sum\limits_{t=1}^{8}\lambda_{5t;1}\tilde{E}_{t;1}=0 \\ \tau_1\big|_{x=x_0}=\sum\limits_{t=1}^{8}\lambda_{6t;1}\tilde{E}_{t;1}=0 \\ -a_{14;1}\dfrac{\partial \phi_1}{\partial x}-a_{15;1}\dfrac{\partial \psi_1}{\partial x}+a_{1;1}\tau_1\Big|_{x=x_0}=\sum\limits_{t=1}^{8}\lambda_{7t;1}\tilde{E}_{t;1}=0 \\ -a_{15;1}\dfrac{\partial \phi_1}{\partial x}-a_{16;1}\dfrac{\partial \psi_1}{\partial x}+a_{2;1}\tau_1\Big|_{x=x_0}=\sum\limits_{t=1}^{8}\lambda_{8t;1}\tilde{E}_{t;1}=0 \end{cases} \tag{40}$$

$$\begin{cases} -a_{13;n}\dfrac{\partial u_n}{\partial x}+a_{4;n}\sigma_n-a_{8;n}D_n-a_{11;n}B_n\Big|_{x=x_n}=\sum\limits_{t=1}^{8}\lambda_{5t;n}\tilde{E}_{t;n}\mathrm{e}^{x_n\eta_{t;n}}=0 \\ \tau_n\big|_{x=x_n}=\sum\limits_{t=1}^{8}\lambda_{6t;n}\tilde{E}_{t;n}\mathrm{e}^{x_n\eta_{t;n}}=0 \\ -a_{14;n}\dfrac{\partial \phi_n}{\partial x}-a_{15;n}\dfrac{\partial \psi_n}{\partial x}+a_{1;n}\tau_n\Big|_{x=x_n}=\sum\limits_{t=1}^{8}\lambda_{7t;n}\tilde{E}_{t;n}\mathrm{e}^{x_n\eta_{t;n}}=0 \\ -a_{15;n}\dfrac{\partial \phi_n}{\partial x}-a_{16;n}\dfrac{\partial \psi_n}{\partial x}+a_{2;n}\tau_n\Big|_{x=x_n}=\sum\limits_{t=1}^{8}\lambda_{8t;n}\tilde{E}_{t;n}\mathrm{e}^{x_n\eta_{t;n}}=0 \end{cases} \tag{41}$$

$$\begin{cases} u_{k+1}\big|_{x=x_k}=u_k\big|_{x=x_k} \\ w_{k+1}\big|_{x=x_k}=w_k\big|_{x=x_k} \\ \phi_{k+1}\big|_{x=x_k}=\phi_k\big|_{x=x_k} \\ \psi_{k+1}\big|_{x=x_k}=\psi_k\big|_{x=x_k} \\ -a_{13;(k+1)}\dfrac{\partial u_{k+1}}{\partial x}+a_{4;(k+1)}\sigma_{k+1}-a_{8;(k+1)}D_{k+1}-a_{11;(k+1)}B_{k+1}\Big|_{x=x_k}=-a_{13;k}\dfrac{\partial u_k}{\partial x}+a_{4;k}\sigma_k-a_{8;k}D_k-a_{11;k}B_k\Big|_{x=x_k} \\ \tau_{k+1}\big|_{x=x_k}=\tau_k\big|_{x=x_k} \\ -a_{14;(k+1)}\dfrac{\partial \phi_{k+1}}{\partial x}-a_{15;(k+1)}\dfrac{\partial \psi_{k+1}}{\partial x}+a_{1;(k+1)}\tau_{k+1}\Big|_{x=x_k}=-a_{14;k}\dfrac{\partial \phi_k}{\partial x}-a_{15;k}\dfrac{\partial \psi_k}{\partial x}+a_{1;k}\tau_k\Big|_{x=x_k} \\ -a_{15;(k+1)}\dfrac{\partial \phi_{k+1}}{\partial x}-a_{16;(k+1)}\dfrac{\partial \psi_{k+1}}{\partial x}+a_{2;(k+1)}\tau_{k+1}\Big|_{x=x_k}=-a_{15;k}\dfrac{\partial \phi_k}{\partial x}-a_{16;k}\dfrac{\partial \psi_k}{\partial x}+a_{2;k}\tau_k\Big|_{x=x_k} \end{cases}$$

which result in

$$\sum_{t=1}^{8}\lambda_{it;(k+1)}\tilde{E}_{t;(k+1)}\mathrm{e}^{x_k\eta_{t;k+1}}=\sum_{t=1}^{8}\lambda_{it;k}\tilde{E}_{t;k}\mathrm{e}^{x_k\eta_{t;k}}\quad(i=1,2,\cdots,8) \tag{42}$$

where

$$\begin{cases} \lambda_{it;k} = \Upsilon_{it;k} \quad (i=1,2,\cdots,4) \\ \lambda_{5t;k} = -a_{13;k}\Upsilon_{1t;k}\eta_{t;k} + a_{4;k}\Upsilon_{5t;k} - a_{8;k}\Upsilon_{6t;k} - a_{11;k}\Upsilon_{7t;k} \\ \lambda_{6t;k} = 1 \\ \lambda_{7t;k} = -a_{14;k}\Upsilon_{3t;k}\eta_{t;k} - a_{15;k}\Upsilon_{4t;k}\eta_{t;k} + a_{1;k} \\ \lambda_{8t;k} = -a_{15;k}\Upsilon_{3t;k}\eta_{t;k} - a_{16;k}\Upsilon_{4t;k}\eta_{t;k} + a_{2;k} \end{cases} \tag{43}$$

As can be seen from Eq. (42), it becomes possible to bridge the gap between the homogeneous boundary conditions present in the first and the n-th layers by

$$\{\tilde{E}_{t;n}\} = \prod_{k=1}^{n-1} [\boldsymbol{\mathcal{L}}_{k+1}^{-1}\boldsymbol{\mathcal{L}}_k]_{x=x_k} \{\tilde{E}_{t;1}\} \tag{44}$$

which leads to the substitution of $\tilde{E}_{t;n}$ with $\tilde{E}_{t;1}$ at $x = x_n$, where $\{\tilde{E}_{t;k}\}$ represents the coefficient vector for $t = 1,2,\cdots,8$; $[\boldsymbol{\mathcal{L}}_k]_{x=x_k}$ is the transfer matrix, the elements of which are $\left([\boldsymbol{\mathcal{L}}_k]_{x=x_k}\right)_{ij} = \lambda_{ij;k}\mathrm{e}^{x_k\eta_{j;k}}$. For nontrivial solutions for $\tilde{E}_{t;1}$ to exist, the determinant of the following matrix ought to vanish:

$$\det\left[\lambda_{(i+4)j;1}\mathfrak{H}(4-i) + \lambda_{ij;n}\mathrm{e}^{x_n\eta_{j;n}}\left\{\prod_{k=1}^{n-1}[\boldsymbol{\mathcal{L}}_{k+1}^{-1}\boldsymbol{\mathcal{L}}_k]_{x=x_k}\right\}_{ij}\mathfrak{H}(i-5)\right] = 0 \quad (i=1,2,\cdots,8; j=1,2,\cdots,8) \tag{45}$$

where $\mathfrak{H}(x)$ is the Heaviside function, defined as

$$\mathfrak{H}(x) = \begin{cases} 1, & x \geq 0 \\ 0, & x < 0 \end{cases} \tag{46}$$

The characteristic equation is expressed in Eq. (45), which determines the eigenvalues $\mu_{i;k}$, where the subscript represents the i-th root of the characteristic equation in the k-th layer. We finally arrive at the eigen-solutions for general eigenvalues:

$$\boldsymbol{f}_{\mu,i;k} = \mathrm{e}^{\mu_{i;k}z}\boldsymbol{\Phi}_{i;k} \tag{47}$$

2.4. Complete solution

It is noted that the global state vectors are piecewise functions, and we denote the global vectors as

$$\boldsymbol{f}_{\mu,i} = \bigcup_{k=1}^{n} \boldsymbol{f}_{\mu,i;k} \tag{48}$$

Through the method of separation of variables, the complete solution of Eq. (5) is derived via symplectic expansion as

$$\begin{aligned}\boldsymbol{f} &= \sum_{i=1}^{10} m_{0,i}\boldsymbol{f}_{0,i} + \sum_{i=1}^{\infty}\left[(m_{\mu,i}^{\mathrm{Re}}\mathrm{Re}\boldsymbol{f}_{\mu,i} + m_{\mu,i}^{\mathrm{Im}}\mathrm{Im}\boldsymbol{f}_{\mu,i}) + (m_{-\mu,i}^{\mathrm{Re}}\mathrm{Re}\boldsymbol{f}_{-\mu,i} + m_{-\mu,i}^{\mathrm{Im}}\mathrm{Im}\boldsymbol{f}_{-\mu,i})\right] \\ &\triangleq \sum_{i=1}^{\infty} m_i\boldsymbol{f}_i\end{aligned} \tag{49}$$

where $\boldsymbol{f}_{0,i}$ $(i=1,2,\cdots,10)$ are the eigen-solutions for zero eigenvalue, $\boldsymbol{f}_{\mu,i}$ and $\boldsymbol{f}_{-\mu,i}$ are the eigen-solutions for general eigenvalues μ_i and $-\mu_i$, respectively; $m_{0,i}$, $m_{\mu,i}^{\mathrm{Re}}$, $m_{\mu,i}^{\mathrm{Im}}$, $m_{-\mu,i}^{\mathrm{Re}}$, and $m_{-\mu,i}^{\mathrm{Im}}$ are the coefficients for superposition; $\mathrm{Re}\,\boldsymbol{f}$ and $\mathrm{Im}\,\boldsymbol{f}$ represent the real and imaginary part of the vector $\boldsymbol{f}$, respectively.

Now, we may take the perfectly insulated frictionless indenter for example. The boundary conditions at $z=h$ and $z=0$ are respectively assumed to be

$$u_k = 0, \quad w_k = 0, \quad \phi_k = 0, \quad \psi_k = 0 \quad (z=h; k=1,2,\cdots,n) \tag{50}$$

$$\begin{cases} w_k = d-\kappa(x) & x\in[\tilde{a},\tilde{b}] \\ \sigma_k = 0 & x\in[x_0,\tilde{a}]\cup[\tilde{b},x_n] \end{cases}, \quad \tau_k = 0, \quad D_k = 0, \quad B_k = 0 \quad (z=0; k=1,2,\cdots,n) \tag{51}$$

where d represents the maximum indentation depth, $\kappa(x)$ is the indenter shape function, and $[\tilde{a},\tilde{b}]$ is the contact region.

The Hamiltonian mixed-energy variational principle (Leung and Zheng, 2007) for the mixed boundary-value problems is given by

$$\begin{aligned}&\delta\left\{\int_0^h\sum_{k=1}^{n}\int_{x_{k-1}}^{x_k}\left[\boldsymbol{p}_k^{\mathrm{T}}\frac{\partial\boldsymbol{q}_k}{\partial z} - H_k(\boldsymbol{q}_k,\boldsymbol{p}_k)\right]\mathrm{d}x\mathrm{d}z - \sum_{k=1}^{n}\int_{\Gamma_{\boldsymbol{q}_h}^k}\left[\boldsymbol{p}_k^{\mathrm{T}}(\boldsymbol{q}_k-\overline{\boldsymbol{q}}_{h;k})\right]\mathrm{d}x\right. \\ &\left. -\sum_{k=1}^{n}\int_{\Gamma_{\boldsymbol{p}_h}^k}\left[\overline{\boldsymbol{p}}_{h;k}^{\mathrm{T}}\boldsymbol{q}_k\right]\mathrm{d}x + \sum_{k=1}^{n}\int_{\Gamma_{\boldsymbol{q}_0}^k}\left[\boldsymbol{p}_k^{\mathrm{T}}(\boldsymbol{q}_k-\overline{\boldsymbol{q}}_{0;k})\right]\mathrm{d}x + \sum_{k=1}^{n}\int_{\Gamma_{\boldsymbol{p}_0}^k}\left[\overline{\boldsymbol{p}}_{0;k}^{\mathrm{T}}\boldsymbol{q}_k\right]\mathrm{d}x\right\} = 0\end{aligned} \tag{52}$$

where $\Gamma_{\boldsymbol{q}_h}^k$ represents the boundary with known displacement $\overline{\boldsymbol{q}}_{h;k}$ at $z=h$ in the k-th layer; $\Gamma_{\boldsymbol{q}_0}^k$, $\Gamma_{\boldsymbol{p}_h}^k$, and $\Gamma_{\boldsymbol{p}_0}^k$ are with similar interpretations to $\Gamma_{\boldsymbol{q}_h}^k$. Given the canonical equations are satisfied within the domain, Eq. (52) is further simplified with substitution of the symplectic

expansion:

$$\begin{aligned}&\sum_{k=1}^{n}\int_{\Gamma_{\boldsymbol{p}_h}^k}\left[(\sum_{i=1}^{\infty}\delta m_i\boldsymbol{q}_{i;k})^{\mathrm{T}}(\sum_{j=1}^{\infty}m_j\boldsymbol{p}_{j;k}-\overline{\boldsymbol{p}}_{h;k})\right]\mathrm{d}x-\sum_{k=1}^{n}\int_{\Gamma_{\boldsymbol{q}_h}^k}\left[(\sum_{i=1}^{\infty}\delta m_i\boldsymbol{p}_{i;k})^{\mathrm{T}}(\sum_{j=1}^{\infty}m_j\boldsymbol{q}_{j;k}-\overline{\boldsymbol{q}}_{h;k})\right]\mathrm{d}x\\&+\sum_{k=1}^{n}\int_{\Gamma_{\boldsymbol{q}_0}^k}\left[(\sum_{i=1}^{\infty}\delta m_i\boldsymbol{p}_{i;k})^{\mathrm{T}}(\sum_{j=1}^{\infty}m_j\boldsymbol{q}_{j;k}-\overline{\boldsymbol{q}}_{0;k})\right]\mathrm{d}x-\sum_{k=1}^{n}\int_{\Gamma_{\boldsymbol{p}_0}^k}\left[(\sum_{i=1}^{\infty}\delta m_i\boldsymbol{q}_{i;k})^{\mathrm{T}}(\sum_{j=1}^{\infty}m_j\boldsymbol{p}_{j;k}-\overline{\boldsymbol{p}}_{0;k})\right]\mathrm{d}x=0\end{aligned}\tag{53}$$

Letting

$$\begin{aligned}\mathscr{A}_{ij}&=\sum_{k=1}^{n}\left\{\int_{\Gamma_{\boldsymbol{p}_h}^k}\left[(\boldsymbol{q}_{i;k})^{\mathrm{T}}\boldsymbol{p}_{j;k}\right]\mathrm{d}x-\int_{\Gamma_{\boldsymbol{q}_h}^k}\left[(\boldsymbol{p}_{i;k})^{\mathrm{T}}\boldsymbol{q}_{j;k}\right]\mathrm{d}x+\int_{\Gamma_{\boldsymbol{q}_0}^k}\left[(\boldsymbol{p}_{i;k})^{\mathrm{T}}\boldsymbol{q}_{j;k}\right]\mathrm{d}x-\int_{\Gamma_{\boldsymbol{p}_0}^k}\left[(\boldsymbol{q}_{i;k})^{\mathrm{T}}\boldsymbol{p}_{j;k}\right]\mathrm{d}x\right\}\\\mathscr{H}_{i}&=\sum_{k=1}^{n}\left\{\int_{\Gamma_{\boldsymbol{p}_h}^k}\left[(\boldsymbol{q}_{i;k})^{\mathrm{T}}\overline{\boldsymbol{p}}_{h;k}\right]\mathrm{d}x-\int_{\Gamma_{\boldsymbol{q}_h}^k}\left[(\boldsymbol{p}_{i;k})^{\mathrm{T}}\overline{\boldsymbol{q}}_{h;k}\right]\mathrm{d}x+\int_{\Gamma_{\boldsymbol{q}_0}^k}\left[(\boldsymbol{p}_{i;k})^{\mathrm{T}}\overline{\boldsymbol{q}}_{0;k}\right]\mathrm{d}x-\int_{\Gamma_{\boldsymbol{p}_0}^k}\left[(\boldsymbol{q}_{i;k})^{\mathrm{T}}\overline{\boldsymbol{p}}_{0;k}\right]\mathrm{d}x\right\}\end{aligned}\tag{54}$$

we obtain

$$\mathscr{A}_{ij}m_j=\mathscr{H}_i\tag{55}$$

The solutions are then derived as

$$m_k=\frac{\det\mathscr{A}_{ij}^k}{\det\mathscr{A}_{ij}}\tag{56}$$

where $\mathscr{A}_{ij}^k$ is the matrix formed by replacing the k-th column of $\mathscr{A}_{ij}$ with the column vector $\mathscr{H}_i$. Till now, we have accomplished the symplectic framework for contact analysis of a horizontally laminated finite specimen.

3. Numerical examples and discussions

3.1. Interfacial effect

To explore the interfacial effect, we give a particular example of the above analysis: a rigid flat-ended punch applied on the surface of a two-phase, purely elastic, rectangular specimen with length $20(\mathrm{m})$ and width $10(\mathrm{m})$, as depicted in Fig. 2. The interface is at $x_1=10(\mathrm{m})$. The Young's modulus of the two phases/layers are taken as $E_1=1(\mathrm{Pa})$ and $E_2=1.1(\mathrm{Pa})$ respectively, but with the same Poisson's ratio $\nu=0.25$. The contact region is

$x \in [9.5,10.5]$ (m), and the maximum indentation depth is $d = 0.02$(m).

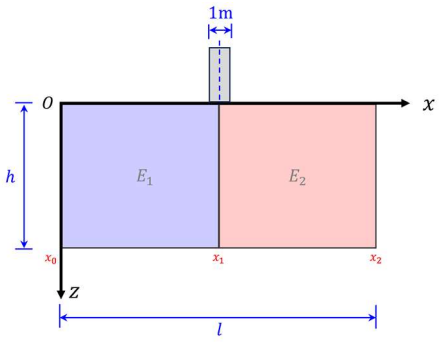

Fig. 2. A rigid flat-ended punch applied symmetrically with respect to the interface (i.e., $x = x_1 = 10$(m)) on the surface of a two-phase, purely elastic, rectangular specimen. The coordinate origin is selected at $O(0,0)$, with $x_0 = 0$ and $x_2 = l$.

The governing state equation for the k-th layer ($k = 1$ or 2) is

$$\frac{\partial}{\partial z}\begin{Bmatrix} u_{z;k} \\ u_{x;k} \\ \sigma_{zz;k} \\ \tau_{xz;k} \end{Bmatrix} = \begin{bmatrix} 0 & -\nu\dfrac{\partial}{\partial x} & \dfrac{1-\nu^2}{E_k} & 0 \\ -\dfrac{\partial}{\partial x} & 0 & 0 & \dfrac{2(1+\nu)}{E_k} \\ 0 & 0 & 0 & -\dfrac{\partial}{\partial x} \\ 0 & -E_k\dfrac{\partial^2}{\partial x^2} & -\nu\dfrac{\partial}{\partial x} & 0 \end{bmatrix} \begin{Bmatrix} u_{z;k} \\ u_{x;k} \\ \sigma_{zz;k} \\ \tau_{xz;k} \end{Bmatrix} \tag{57}$$

The homogeneous boundary conditions at $x = x_0$ and $x = x_2$ are

$$\begin{aligned} &\left(E_1\frac{\partial u_{x;1}}{\partial x} + \nu\sigma_{zz;1} = 0\right)\Big|_{x=x_0} = 0, \quad \sigma_{xz;1}\big|_{x=x_0} = 0 \\ &\left(E_2\frac{\partial u_{x;2}}{\partial x} + \nu\sigma_{zz;2} = 0\right)\Big|_{x=x_2} = 0, \quad \sigma_{xz;2}\big|_{x=x_2} = 0 \end{aligned} \tag{58}$$

Moreover, the displacements and stresses at the interface should satisfy the continuity conditions:

$$\begin{cases} u_{x;k}(x_k) = u_{x;(k+1)}(x_k), & u_{z;k}(x_k) = u_{z;(k+1)}(x_k) \\ \sigma_{xx;k}(x_k) = \sigma_{xx;(k+1)}(x_k), & \sigma_{xz;k}(x_k) = \sigma_{xz;(k+1)}(x_k) \end{cases} \tag{59}$$

where $\sigma_{mn;k}$ are the stress components; $u_{x;k}$ and $u_{z;k}$ are the displacement components in the x- and z-directions, respectively. The boundary conditions at the lower and upper surfaces are:

$$z=h,\quad \begin{cases} u_{z;k}=0 \\ u_{x;k}=0 \end{cases};\quad z=0,\quad \begin{cases} \sigma_{xz;k}=0 & x\in[x_0,x_2] \\ u_{z;k}=d & x\in[a,b] \\ \sigma_{zz;k}=0 & x\in[x_0,a]\cup[b,x_2] \end{cases} \qquad (k=1,2) \tag{60}$$

It is noted here that the specimen is assumed to be fixed to the rigid substrate at the lower surface.

Through the method of separation of variables, the eigen-solutions for zero eigenvalue are obtained as

$$\begin{aligned} &\boldsymbol{f}_{0,s;k}^{(0)}=\boldsymbol{\Phi}_{0,s;k}^{(0)}=[1,0,0,0]^{\mathrm{T}}, && \boldsymbol{f}_{0,a;k}^{(0)}=\boldsymbol{\Phi}_{0,a;k}^{(0)}=[0,1,0,0]^{\mathrm{T}} \\ &\boldsymbol{f}_{0,s;k}^{(1)}=\boldsymbol{\Phi}_{0,s;k}^{(1)}+z\boldsymbol{\Phi}_{0,s;k}^{(0)}=[z,-\nu x+\zeta_1,E_k,0]^{\mathrm{T}}, && \boldsymbol{f}_{0,a;k}^{(1)}=\boldsymbol{\Phi}_{0,a;k}^{(1)}+z\boldsymbol{\Phi}_{0,a;k}^{(0)}=[-x+\zeta_2,z,0,0]^{\mathrm{T}} \\ &\boldsymbol{f}_{0,a;k}^{(2)}=\boldsymbol{\Phi}_{0,a;k}^{(2)}+z\boldsymbol{\Phi}_{0,a;k}^{(1)}+\frac{z^2}{2}\boldsymbol{\Phi}_{0,a;k}^{(0)}=[(-x+\zeta_2)z,\frac{1}{2}[\nu(x-\zeta_2)^2+z^2]+\zeta_3,-E_k(x-\zeta_2),0]^{\mathrm{T}} \\ &\boldsymbol{f}_{0,a;k}^{(3)}=\boldsymbol{\Phi}_{0,a;k}^{(3)}+z\boldsymbol{\Phi}_{0,a;k}^{(2)}+\frac{z^2}{2!}\boldsymbol{\Phi}_{0,a;k}^{(1)}+\frac{z^3}{3!}\boldsymbol{\Phi}_{0,a;k}^{(0)} \end{aligned} \tag{61}$$

where the subscripts s and a represent symmetric and antisymmetric solutions, respectively; and

$$\boldsymbol{\Phi}_{0,a;k}^{(3)}=\begin{Bmatrix} \dfrac{2(1+\nu)}{6}(x-\zeta_2)^3+\left[\dfrac{2(1+\nu)}{E_k}-\zeta_3\right](x-\zeta_2)+\beta_{3k}+\zeta_4 \\ 0 \\ 0 \\ \dfrac{E_k}{2}(x-\zeta_2)^2+\beta_{1k} \end{Bmatrix} \tag{62}$$

where β_{1k} and β_{3k} can be derived through the continuity conditions recursively; ζ_1,ζ_2,ζ_3, and ζ_4 are determined with the symplectic orthogonal relations between the eigenvectors, which are given in Appendix D.

While for nonzero eigenvalues, the corresponding eigen-solutions can be expressed as

$$\begin{cases} u_{z,n;k}=\mathcal{A}_{1n;k}\cos(\mu_n x)+\mathcal{A}_{2n;k}\sin(\mu_n x)+\mathcal{A}_{3n;k}x\sin(\mu_n x)+\mathcal{A}_{4n;k}x\cos(\mu_n x) \\ u_{x,n;k}=\mathcal{B}_{1n;k}\sin(\mu_n x)+\mathcal{B}_{2n;k}\cos(\mu_n x)+\mathcal{B}_{3n;k}x\cos(\mu_n x)+\mathcal{B}_{4n;k}x\sin(\mu_n x) \\ \sigma_{zz,n;k}=\mathcal{C}_{1n;k}\cos(\mu_n x)+\mathcal{C}_{2n;k}\sin(\mu_n x)+\mathcal{C}_{3n;k}x\sin(\mu_n x)+\mathcal{C}_{4n;k}x\cos(\mu_n x) \\ \sigma_{xz,n;k}=\mathcal{D}_{1n;k}\sin(\mu_n x)+\mathcal{D}_{2n;k}\cos(\mu_n x)+\mathcal{D}_{3n;k}x\cos(\mu_n x)+\mathcal{D}_{4n;k}x\sin(\mu_n x) \end{cases} \tag{63}$$

where $\mathcal{A}_{in}$, $\mathcal{B}_{in}$, $\mathcal{C}_{in}$, and $\mathcal{D}_{in}$ are constants, the relations of which are clarified in Appendix D. Furthermore, the following characteristic equation, which is depicted numerically in Fig. 3, is

derived through the homogeneous boundary conditions together with the transfer matrix:

$$\begin{aligned}
&\frac{1}{32E_1^2\mu^2}\Big\{2E_1^2\left(2\mu^2x_1^2-1\right)\left(-(\nu-2)\nu+2\mu^2(\nu+1)^2x_1^2-4\mu^2(\nu+1)^2x_1x_2+2\mu^2(\nu+1)^2x_2^2-5\right)\\
&+2(E_1-E_2)\cos(2\mu x_1)\Big[E_1\left(-(\nu-2)\nu+2\mu^2(\nu+1)^2x_1^2-4\mu^2(\nu+1)^2x_1x_2+2\mu^2(\nu+1)^2x_2^2-5\right)\\
&-E_2(\nu-3)(\nu+1)\left(2\mu^2(x_1-x_2)^2-1\right)\Big]+2E_2^2\left(-(\nu-2)\nu+2\mu^2(\nu+1)^2x_1^2-5\right)\left(2\mu^2(x_1-x_2)^2-1\right)\\
&+2(E_1-E_2)\cos(2\mu(x_1-x_2))\Big[E_1(\nu-3)(\nu+1)\left(2\mu^2x_1^2-1\right)+E_2\left((\nu-2)\nu-2\mu^2(\nu+1)^2x_1^2+5\right)\Big]\\
&-4E_1E_2\Big[-2\nu+2\mu^2\left(2\mu^2x_1^2(x_1-x_2)^2-6x_1^2+6x_1x_2+x_2^2\right)+\nu^2\left(2\mu^2x_1^2-1\right)\left(2\mu^2(x_1-x_2)^2-1\right)\\
&+8\mu^4\nu x_1^2(x_1-x_2)^2+1\Big]+(E_1(\nu+1)-E_2(\nu-3))(E_1(\nu-3)-E_2(\nu+1))\cos(2\mu x_2)\\
&+(\nu-3)(\nu+1)(E_1-E_2)^2\cos(4\mu x_1-2\mu x_2)\Big\}=0
\end{aligned} \tag{64}$$

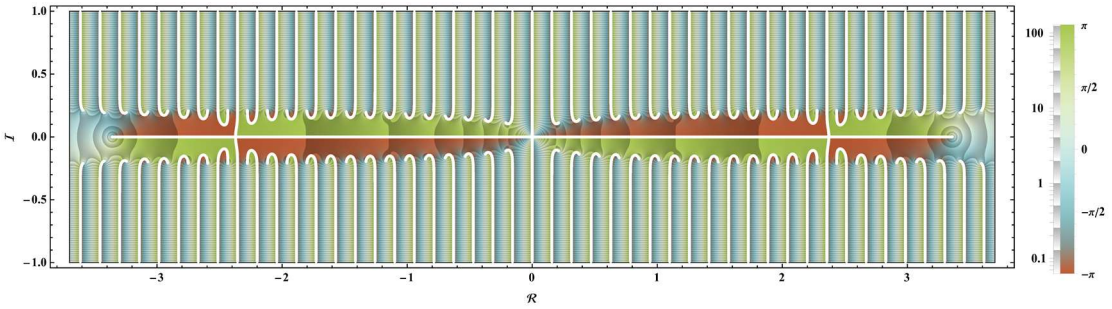

Fig. 3. The distribution of the left-hand side of Eq. (64) on the complex plane (real axis $\Re(\mu)\in[-3.7,3.7]$ and imaginary axis $\Im(\mu)\in[-1,1]$).

From the distributions of the zeros and branch points demonstrated in Fig. 3, we discern a symmetrical pattern of the roots with respect to the real and imaginary axes, except for the multiple zero at the coordinate origin. The roots may be categorized into two categories, i.e., $\{\mu_n,\mu_n^*\}$ and $\{-\mu_n,-\mu_n^*\}$ accordingly, which are denoted as $\widetilde{\alpha}$-set and $\widetilde{\beta}$-set respectively. Here the complex conjugation of μ is represented by μ^*. It is important to highlight that the real part of the root exhibits a periodical pattern, with the specific period being ascertainable through the analysis of the characteristic equation, approximately as $\pi/20$. In addition, all the branch points are located along the real axis, aligning with the presence of the square root terms. The absolute value of the imaginary part initially increases and then decreases between the multiple zero and branch points, before gradually increasing beyond the branch points.

Upon substituting the roots into the eigen-solutions, we arrive at the analytical solution, as illustrated in Fig. 4, where the results from finite element analysis (FEA) are also given for comparison.

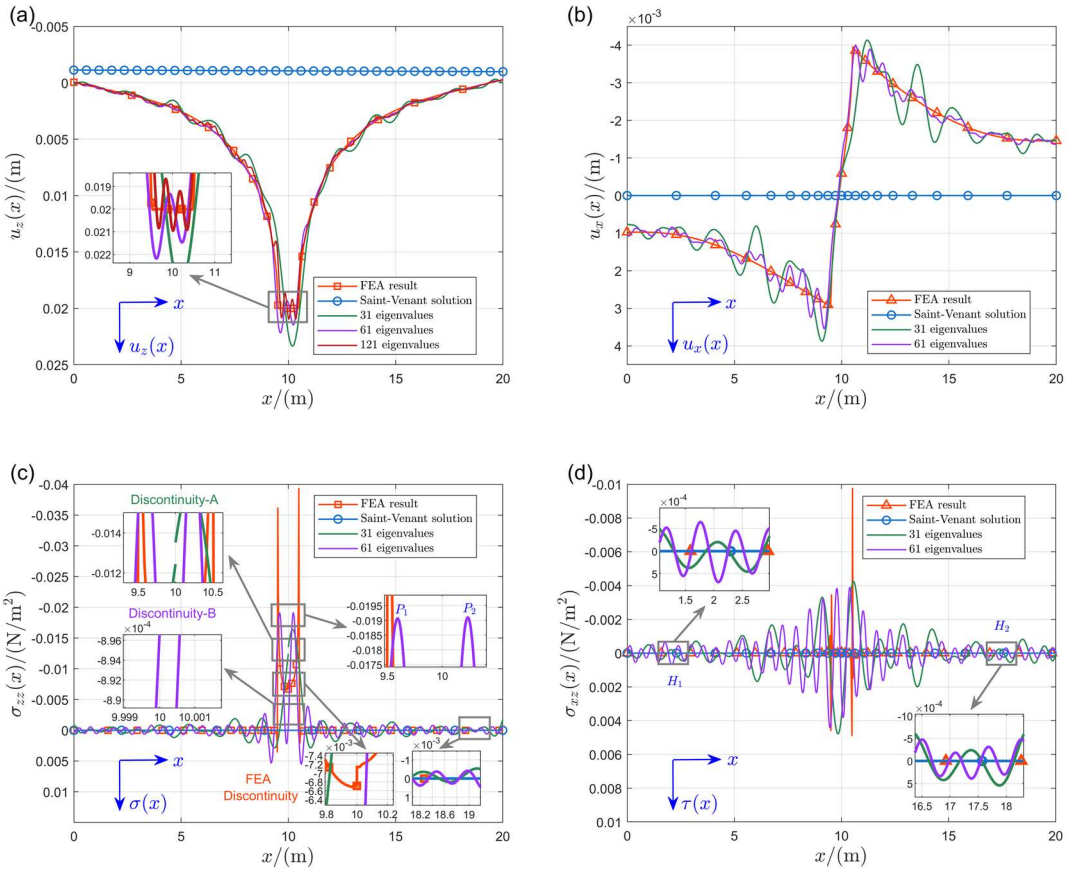

Fig. 4. Comparison between FEA results and analytical solutions on the surface along the x-axis when the flat-ended punch is applied symmetrically with respect to the interface. **(a)** Vertical displacement; **(b)** Horizontal displacement; **(c)** Normal stress; **(d)** Shear stress. To demonstrate the relations among the curves, (a), (c), and (d) are locally enlarged.

The Saint-Venant solutions displayed in Figs. 4(a) and 4(b) reveal the existence of non-exponential decay, while the corresponding terms are absent in the stress expressions. It is worth noting that the upward displacement appearing in the vertical direction is comprehensible, which is physically similar to the elevation of water level when an object is partially submerged

into water. In addition, the asymmetry with respect to the interface caused by the difference in Young's modulus is also exhibited in Fig. 4(a), i.e., the surface of the softer phase (i.e., $x \in [x_0, x_1]$) rises higher, which can be elucidated through the negative correlation between E_k and the vertical displacement presented in the eigenvector $\boldsymbol{\Phi}_{0,a;k}^{(3)}$.

Furthermore, a notable phenomenon observed across all symplectic solutions is the oscillatory behavior. Without loss of generality, we may take the case with 61 eigenvalues displayed in Fig. 4(d) into account. For brevity, the analytical solutions derived with 61 eigenvalues involved are denoted as "61 eigenvalues". As we can see, the two points H_1 and H_2 are with the lowest amplitude within $x \in [x_0, x_1]$ and $x \in [x_1, x_2]$ respectively, which are taken as the cut-off points to divide the whole region into three parts. The oscillating in curves near the lateral boundaries results from the inherent geometric singularities, and the stress concentration leads to the occurrence of oscillation within $x \in [x_{H_1}, x_{H_2}]$. Moreover, this particular property is also exhibited in other state variables, for instance, as enlarged in Fig. 4(c).

The state variables outlined in Eq. (59) are continuous at the interface, whereas the normal stress in the z-direction depicted in Fig. 4(c) exhibits discontinuities at $x = x_1$ (i.e., Discontinuity-A and -B in the analytical solutions with 31 and 61 eigenvalues, respectively), both of which are caused by the abrupt change in Young's modulus. The discontinuity aligns with the findings from FEA (i.e., FEA-Discontinuity), yet the accuracy is compromised by the oscillation. To enhance the prediction accuracy of the position where discontinuity occurs, stress averaging is required to approximate the value at discontinuity, particularly when the number of eigen-solutions for superposition is limited. However, the predicted discontinuities will

converge as adequate eigenvalues are involved. Despite the discontinuity, when the punch is pressed to a certain depth at the interface, the stresses on the relatively softer side are lower than on that on the harder side, which is generally consistent with the physical reality (e.g., the peak P_1 is lower than the peak P_2).

It is crucial to underscore the intricacy of analyzing flat punch problem, particularly when compared with smooth indenters. The distinctive feature of a flat punch lies in its two cusps, which are prone to triggering the Gibbs phenomenon. Additionally, this phenomenon manifests not only in displacements but also in stresses at singularities. To elaborate, the Gibbs phenomenon is an overshoot of the eigenfunction series occurring at a simple discontinuity. However, the application of the flat punch avoids the complexity of determining the contact region during indentation.

The following technique has been applied to diminish the error on account of the large number calculations when the eigenvalues with positive real part occur:

$$\begin{aligned}\boldsymbol{f} &= \sum_{i=1}^{10} m_{0,i}\boldsymbol{f}_{0,i} + \sum_{i=1}^{\infty}\left[(m_{\mu,i}^{\mathrm{Re}}\mathrm{Re}\boldsymbol{f}_{\mu,i} + m_{\mu,i}^{\mathrm{Im}}\mathrm{Im}\boldsymbol{f}_{\mu,i}) + (m_{-\mu,i}^{\mathrm{Re}}\mathrm{Re}\boldsymbol{f}_{-\mu,i} + m_{-\mu,i}^{\mathrm{Im}}\mathrm{Im}\boldsymbol{f}_{-\mu,i})\right] \\ &\equiv \sum_{i=1}^{10} m_{0,i}\boldsymbol{f}_{0,i} + \sum_{i=1}^{\infty}\left\{\left[\tilde{m}_{\mu,i}^{\mathrm{Re}}\mathrm{Re}(\mathrm{e}^{-\mu h}\boldsymbol{f}_{\mu,i}) + \tilde{m}_{\mu,i}^{\mathrm{Im}}\mathrm{Im}(\mathrm{e}^{-\mu h}\boldsymbol{f}_{\mu,i})\right] + (m_{-\mu,i}^{\mathrm{Re}}\mathrm{Re}\boldsymbol{f}_{-\mu,i} + m_{-\mu,i}^{\mathrm{Im}}\mathrm{Im}\boldsymbol{f}_{-\mu,i})\right\}\end{aligned} \tag{65}$$

The results of the FEA simulation are presented in Fig. 5. Notably, the contours indicate that the left part is of significant deformation and relatively low stress level, in contrast to the right part at the same depth, thus exhibiting asymmetry with respect to the interface. Meanwhile, the interfacial effect is also demonstrated, particularly in Fig. 5(c), with the discontinuities displayed at $x = x_1$. Additionally, the stress contours exhibit a more concentrated distribution in the contact region compared to the displacement contours, aligning with the fact that non-exponential decay terms are absent in stresses.

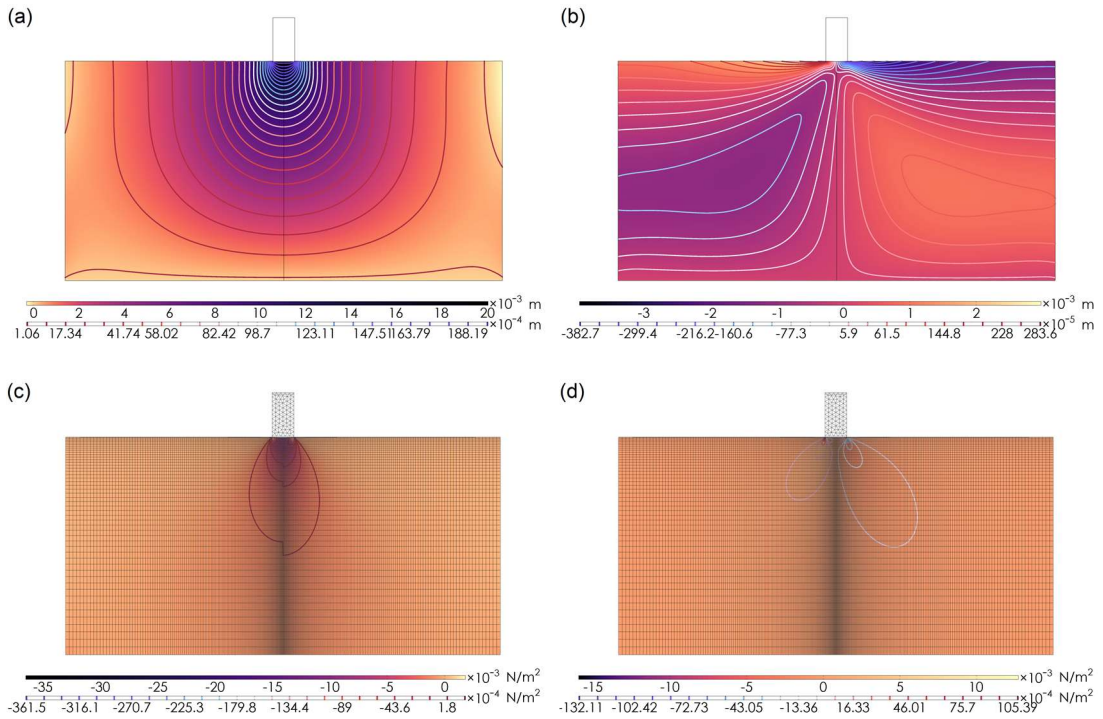

Fig. 5. FEA simulation results for deformations and stress distributions with a rigid flat punch applied symmetrically about the interface on the surface of the horizontally laminated planerectangular specimen. **(a)** Vertical displacement. **(b)** Horizontal displacement. **(c)** Normal stress. **(d)** Shear stress. Meshes with 15431 nodes are refined near the surface, (especially within the contact region), are adopted, as shown in (c) and (d). The meshes for the case of displacements remain are identicalthe same, which are omitted in (a) and (b). The augmented Lagrangian method (ALM) is employed to conduct the contact analyses in COMSOL (COMSOL, 2021), which transforms a constrained optimization problem into a sequence of unconstrained problems and adds a penalty term together with another quasi-Lagrange multiplier term to the objective function.

With a considerable number of layers involved, the laminated model may be used to approximate the specimen with an arbitrary horizontal material gradient. It is worth noting that warping of the plane is not negligible especially when the elastic properties between the layers differ remarkably. To describe the warpage, we should employ the governing equations for the generalized plane-strain model instead, as shown in Appendix D.

3.2. Boundary effect

Apart from the interfacial effect as illustrated in the previous section, we can also investigate the boundary effect through the developed contact analysis framework. Consider a flat-ended punch applied on the surface of a horizontally laminated isotropic specimen near the left lateral boundary. All the parameters are taken to be the same as in Section 3.2, except for the contact region, which is replaced by $x \in [0.5,1.5]$ (m), as depicted in Fig. 6.

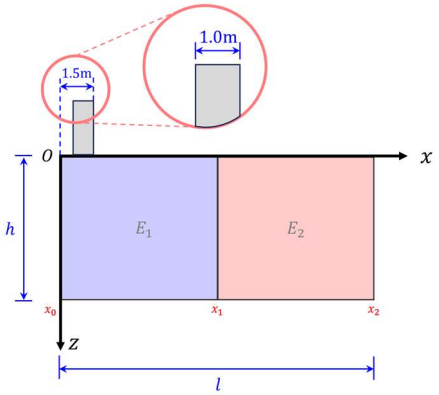

Fig. 6. A rigid flat punch applied on the surface of a horizontally laminated isotropic rectangular specimen near the left lateral boundary. The coordinate origin is chosen at $O(0,0)$, with $x_0 = 0$ and $x_2 = l$.

The analytical solutions along with the FEA results have been obtained and presented in Fig. 7. Evidently, the inclusion of a sufficient number of eigen-solutions leads to precise results, as exemplified by the comparison in Fig. 7(a) between the results for 121 eigenvalues and those for 61 eigenvalues. As for the Saint-Venant solutions, we observe a significant asymmetry in the vertical displacement of the indenter acting close to the boundary, as compared to previous example. Furthermore, we find that the slope of vertical displacement of Saint-Venant solutions is larger than that in the previous example, which is also a consequence of the boundary effect.

Moreover, given the same indentation depth, the resulting stress including the stress concentration of the indenter acting near the lateral boundary is notably lower than that applied centrally, as can be seen from the comparison between Fig. 7(c) and Fig. 4(c), which is referred to as the phenomenon of stress weakening. It is comprehensive that the resistance against the deformation near the left lateral boundary is lower.

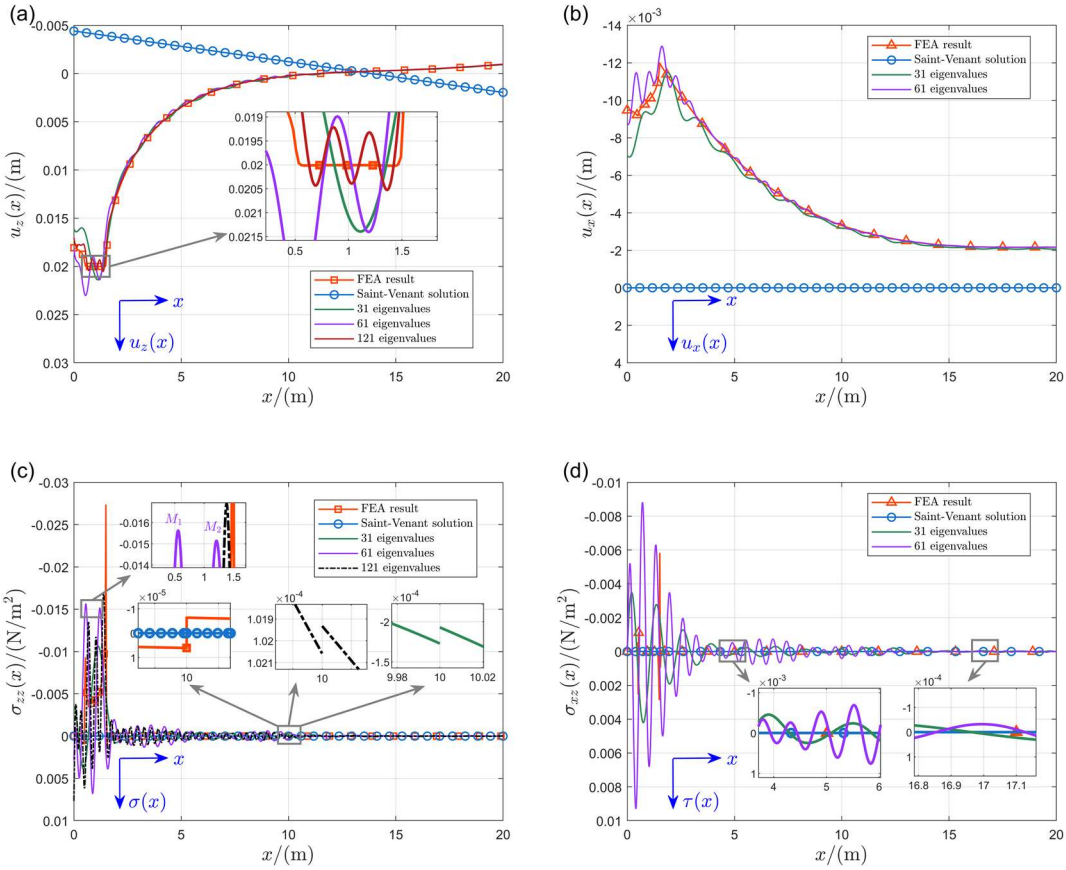

Fig. 7. Comparison between FEA results and analytical solutions on the surface along the x-axis, when the flat punch is applied within $x \in [0.5,1.5]$ (m). **(a)** Vertical displacement. **(b)** Horizontal displacement. **(c)** Normal stress. **(d)** Shear stress. The figures labeled (a), (c), and (d) have been locally enlarged for a detailed display of the curves.

In addition to the above peculiar phenomena, the boundary effect is observed through not only the asymmetrical stress distributions and stress concentrations about $x = 1$ in Figs. 7(c)

and (d), but also the asymmetry behavior in the vertical displacement with respect to the indenter axis, as enlarged in Fig. 7(a). It is noted that the asymmetrical distributions of stresses and displacements do not stem from the inhomogeneity of the laminated specimen, since the indenter is applied far away from the other layer.

The presence of geometric singularity in the left lateral boundary affects the accuracy of the solution. However, the accuracy can be improved as more eigen-solutions are involved. As evident from Fig. 7(d), when the indenter is applied near the geometric singularity, oscillations of the stress and displacement are relatively high, which indicates the oscillating behavior is exacerbated by the geometric singularity. For instance, the oscillation observed in Fig. 7(d) is larger than that in Fig. 4(d). Furthermore, the oscillatory behavior may lead to the error in the prediction of stress concentration. As presented in Fig. 7(c), the analytical solution derived with 61 eigenvectors differs obviously from the FEA simulation (i.e., peak M_1 is higher than M_2). The inefficiency in accurately capturing singularities and stress concentration characterization is primarily due to the insufficient number of eigen-solutions used in superposition. It is also featured by the large oscillation period in the existing eigenvectors. Nevertheless, oscillations can be diminished if an ample number of eigenvalues are involved, while the Gibbs phenomenon still presents, as demonstrated in Fig. 7(c). Overall, the precision will be enhanced with the superposition of adequate number of eigenvectors.

The FEA results are displayed in Fig. 8. The vertical displacements at the bottom are small but negative, which coincides with the Saint-Venant solutions, as depicted in Fig. 8(a). It is important to note that the Saint-Venant solution is conspicuously demonstrated here, whereas in the previous example, the magnitude of which is insufficient to be discernible within

specific contours. The contours are clustered near the left lateral boundary, which is a common feature exhibiting among all the FEA results.

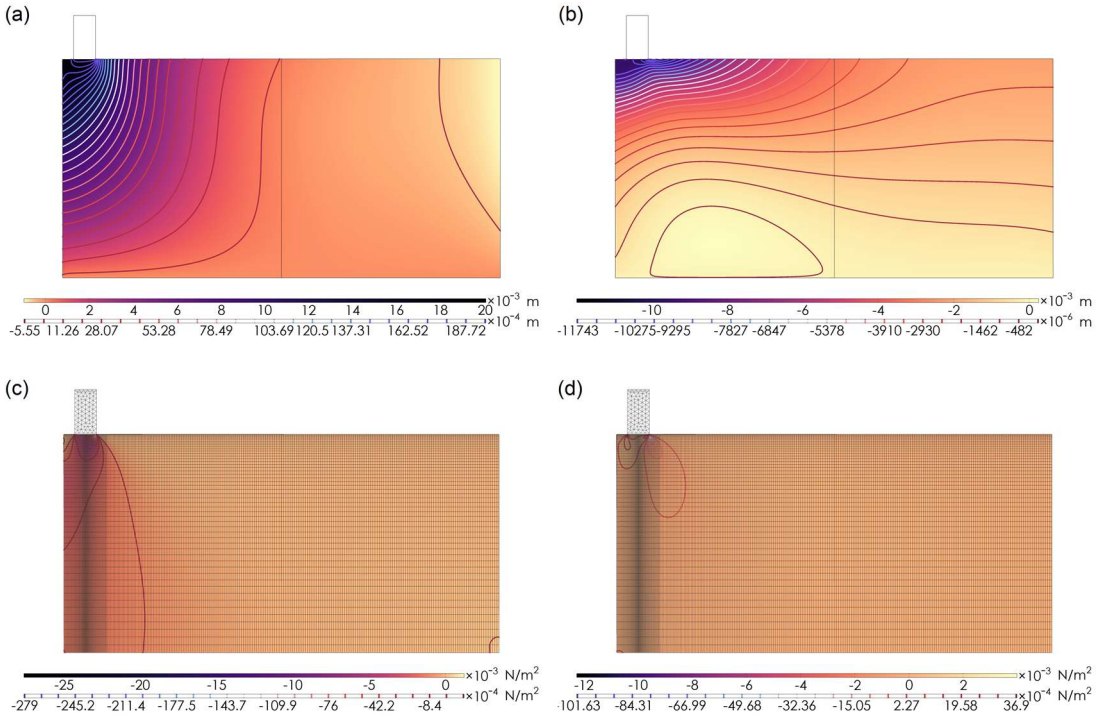

Fig. 8. FEA simulation results for deformations and stress distributions when a rigid flat punch is applied on the surface of the horizontally laminated rectangular specimen at $x \in [0.5,1.5]$. **(a)** Vertical displacement. **(b)** Horizontal displacement. **(c)** Normal stress. **(d)** Shear stress. Meshes with 14411 nodes refined near the surface (especially within the contact region) are adopted, as shown in (c) and (d). The meshes for displacements are identical, which are omitted in (a) and (b). The ALM is employed to solve the contact problems in COMSOL (COMSOL, 2021).

4. Conclusions

In this work, the symplectic framework for contact analysis of a horizontally laminated magneto-electro-elastic finite specimen has been established. The dual variables are involved to establish the canonical equations, which lead to the Hamiltonian operator matrix in the symplectic space. The eigenvectors of the eigenvalue problem are mutually adjoint symplectic-orthogonal, and are associated with the homogeneous lateral boundary conditions and the

continuity conditions at the interfaces. Analytical derivations of the eigenvectors and the corresponding eigen-solutions for zero eigenvalue are conducted for four Jordan chains, which construct a symplectic subspace. The coefficient θ_1, which is introduced in our derivation, plays a pivotal role in fulfilling the constraints of the state variable τ with regard to symplectic orthogonality. For the general eigenvalues, the transfer matrices are deduced to bridge the gap between the boundary conditions across distinct layers, contributing significantly to the determination of the characteristic equation and eigenvectors, and even the respective eigen-solutions. Furthermore, the Hamiltonian mixed energy variational principle is presented and generalized for laminated media, enabling the identification of coefficients in the symplectic expansion. To circumvent the complexity of complex operations in the mixed-boundary value problem, the symplectic expansion is transformed into a real expression by reassembling the eigenvalues in the $\widetilde{\alpha}$-set and $\widetilde{\beta}$-set. It is important to note that the contact analysis is conducted within a finite plane (i.e., a rectangular specimen), providing a more realistic approximation compared to the traditional analytical solutions based on a half-plane. Additionally, with a known contact region, the theory is applicable to indenters with arbitrary profiles. It is noted that, the symplectic framework proposed here surmounts a series of difficulties in dealing with horizontally laminated media, in particular to fulfill the continuity conditions at the interfaces.

The interfacial and boundary effects are discussed in the numerical examples. An intriguing phenomenon is discerned in the Saint-Venant solutions, which becomes comprehensible through the analogy of water surface. The oscillatory behaviors arising from the Gibbs phenomenon and geometric singularity are elucidated. The discontinuity and asymmetrical stress distributions

occurring at the interface are clarified. Furthermore, the stress weakening phenomenon and the asymmetric characteristics of the state variables with respect to the indenter axis are explored in the boundary effect. With sufficient eigen-solutions in superposition, the analytical solutions become highly precise, as validated by the FEA simulations.

It is noted that, when a considerable number of layers are involved, the laminated model considered here has the capability to approximate a plane with any desired horizontal material gradient. In another word, the framework can also be applied to a functionally graded specimen, which has become increasingly popular in HTC. In summary, the symplectic approach has proven its efficacy in addressing hitherto unresolved issues pertaining to contact analysis, laying a solid foundation for subsequent research endeavors in this area.

CRediT authorship contribution statement

Lizichen Chen: Writing – original draft, Validation, Methodology, Investigation, Conceptualization. **Weiqiu Chen**: Writing – review & editing, Supervision, Funding acquisition.

Acknowledgments

The work was supported by the National Natural Science Foundation of China (Nos. 12192211 and 12192210) and the 111 Project, PR China (No. B21034). This work was also partly supported by the specialized research projects of Huanjiang Laboratory, Zhuji, Zhejiang Province.

Appendix A. Constants in basic formulations

$$
\begin{aligned}
a_{1;k} &= e_{15;k} \,/\, c_{44;k}, \\
a_{4;k} &= (c_{13;k} b_{1;k} + e_{31;k} b_{2;k} + q_{31;k} b_{3;k}) \,/\, b_{0;k}, \\
a_{7;k} &= b_{3;k} \,/\, b_{0;k}, \\
a_{10;k} &= b_{5;k} \,/\, b_{0;k}, \\
a_{13;k} &= -c_{11;k} + c_{13;k} a_{4;k} - e_{31;k} a_{8;k} - q_{31;k} a_{11;k}, \\
a_{16;k} &= \gamma_{11;k} + q_{15;k}^2 \,/\, c_{44;k}, \\
a_{19;k} &= q_{31;k} \,/\, c_{11;k}, \\
b_{2;k} &= e_{33;k} \gamma_{33;k} - q_{33;k} d_{33;k}, \\
b_{5;k} &= c_{33;k} d_{33;k} + e_{33;k} q_{33;k}, \\
g_{1;k} &= (a_{9;k} a_{12;k} - a_{10;k}^2) \,/\, g_{0;k}, \\
g_{4;k} &= (a_{5;k} a_{10;k} - a_{6;k} a_{7;k}) \,/\, g_{0;k}, \\
g_{7;k} &= -a_{4;k} g_{1;k} + a_{8;k} g_{2;k} + a_{11;k} g_{3;k}, \\
\rho_{1;k} &= a_{17;k} g_{7;k} + g_{1;k}, \\
\rho_{4;k} &= a_{18;k} g_{7;k} + g_{2;k}, \\
\rho_{7;k} &= a_{19;k} g_{7;k} + g_{3;k}, \\
\rho_{10;k} &= a_{15;k}^2 - a_{14;k} a_{16;k}, \\
\rho_{13;k} &= [a_{15;k}(a_{1;k}\rho_{1;k} - \rho_{2;k}) - a_{14;k}(a_{2;k}\rho_{1;k} - \rho_{3;k})] \,/\, \rho_{10;k}, \\
\rho_{16;k} &= a_{1;k}\rho_{12;k} + a_{2;k}\rho_{14;k} - a_{3;k}\tilde{\beta}_{5;k} + \tilde{\beta}_{4;k}
\end{aligned}
$$

$$
\begin{aligned}
a_{2;k} &= q_{15;k} \,/\, c_{44;k}, \\
a_{5;k} &= b_{1;k} \,/\, b_{0;k}, \\
a_{8;k} &= (-c_{13;k} b_{2;k} + e_{31;k} b_{4;k} - q_{31;k} b_{5;k}) \,/\, b_{0;k}, \\
a_{11;k} &= (-c_{13;k} b_{3;k} + q_{31;k} b_{6;k} - e_{31;k} b_{5;k}) \,/\, b_{0;k}, \\
a_{14;k} &= \varepsilon_{11;k} + e_{15;k}^2 \,/\, c_{44;k}, \\
a_{17;k} &= c_{13;k} \,/\, c_{11;k}, \\
b_{0;k} &= c_{33;k} b_{1;k} + e_{33;k} b_{2;k} + q_{33;k} b_{3;k}, \\
b_{3;k} &= \varepsilon_{33;k} q_{33;k} - e_{33;k} d_{33;k}, \\
b_{6;k} &= c_{33;k} \varepsilon_{33;k} + e_{33;k}^2, \\
g_{2;k} &= (a_{6;k} a_{12;k} + a_{7;k} a_{10;k}) \,/\, g_{0;k}, \\
g_{5;k} &= (a_{5;k} a_{12;k} + a_{7;k}^2) \,/\, g_{0;k}, \\
g_{8;k} &= a_{4;k} g_{2;k} + a_{8;k} g_{5;k} + a_{11;k} g_{4;k}, \\
\rho_{2;k} &= -a_{17;k} g_{8;k} + g_{2;k}, \\
\rho_{5;k} &= -a_{18;k} g_{8;k} - g_{5;k}, \\
\rho_{8;k} &= -a_{19;k} g_{8;k} - g_{4;k}, \\
\rho_{11;k} &= [a_{16;k}(a_{1;k}\rho_{1;k} - \rho_{2;k}) + a_{15;k}(a_{2;k}\rho_{1;k} - \rho_{3;k})] \,/\, \rho_{10;k}, \\
\rho_{14;k} &= [a_{15;k}(a_{1;k}\tilde{\beta}_{5;k} + \tilde{\beta}_{6;k}) - a_{14;k}(a_{2;k}\tilde{\beta}_{5;k} + \tilde{\beta}_{7;k})] \,/\, \rho_{10;k},
\end{aligned}
$$

$$
\begin{aligned}
a_{3;k} &= 1 \,/\, c_{44;k} \\
a_{6;k} &= b_{2;k} \,/\, b_{0;k} \\
a_{9;k} &= b_{4;k} \,/\, b_{0;k} \\
a_{12;k} &= b_{6;k} \,/\, b_{0;k} \\
a_{15;k} &= d_{11;k} + e_{15;k} q_{15;k} \,/\, c_{44;k} \\
a_{18;k} &= e_{31;k} \,/\, c_{11;k} \\
b_{1;k} &= \gamma_{33;k} \varepsilon_{33;k} - d_{33;k}^2 \\
b_{4;k} &= c_{33;k} \gamma_{33;k} + q_{33;k}^2 \\
g_{0;k} &= a_{5;k}(a_{9;k} a_{12;k} - a_{10;k}^2) + a_{6;k}(a_{6;k} a_{12;k} + a_{7;k} a_{10;k}) \\
&\quad + a_{7;k}(a_{6;k} a_{10;k} + a_{7;k} a_{9;k}) \\
g_{3;k} &= (a_{6;k} a_{10;k} + a_{7;k} a_{9;k}) \,/\, g_{0;k} \\
g_{6;k} &= (a_{5;k} a_{9;k} + a_{6;k}^2) \,/\, g_{0;k} \\
g_{9;k} &= a_{4;k} g_{3;k} + a_{8;k} g_{4;k} + a_{11;k} g_{6;k} \\
\rho_{3;k} &= -a_{17;k} g_{9;k} + g_{3;k} \\
\rho_{6;k} &= -a_{18;k} g_{9;k} - g_{4;k} \\
\rho_{9;k} &= -a_{19;k} g_{9;k} - g_{6;k} \\
\rho_{12;k} &= [a_{16;k}(a_{1;k}\tilde{\beta}_{5;k} + \tilde{\beta}_{6;k}) + a_{15;k}(a_{2;k}\tilde{\beta}_{5;k} + \tilde{\beta}_{7;k})] \,/\, \rho_{10;k} \\
\rho_{15;k} &= a_{1;k}\rho_{11;k} + a_{2;k}\rho_{13;k} - a_{3;k}\rho_{1;k} + a_{17;k}
\end{aligned}
$$

Appendix B. Parameters selection and satisfaction of lateral boundary conditions

In the symplectic analysis for zero eigenvalue, we observe that the eigen equation is formulated by a system of first-order differential equations concerning the forms of boundary conditions; the last four equations in Eq. (18) may be rewritten as

$$-\frac{\partial \sigma_{xx;k}}{\partial x}=0,\quad -\frac{\partial \sigma_{xz;k}}{\partial x}=0,\quad -\frac{\partial D_{x;k}}{\partial x}=0,\quad -\frac{\partial B_{x;k}}{\partial x}=0 \tag{B.1}$$

The eight boundary conditions are,

$$\sigma_{xx;1}(x_0)=0,\quad \sigma_{xz;1}(x_0)=0,\quad D_{x;1}(x_0)=0,\quad B_{x;1}(x_0)=0 \tag{B.2}$$

$$\sigma_{xx;n}(x_n)=0,\quad \sigma_{xz;n}(x_n)=0,\quad D_{x;n}(x_n)=0,\quad B_{x;n}(x_n)=0 \tag{B.3}$$

We can then first solve for the four variables in the first layer via Eqs. (B.1) and (B.2). Nevertheless, constraints on the rest variables in $\boldsymbol{q}$ (i.e., $u_{x;k}$, $u_{z;k}$, φ_k, and ψ_k should be continuous across the interface) are absent, which lead to the undetermined constants in Jordan form eigenvectors. Through continuity conditions, the variables in subsequent layers are derived. However, the Jordan form eigenvectors may not fulfill the boundary conditions at $x=x_n$ shown in Eq. (B.3). We can make the satisfaction of boundary conditions by determining the undetermined constants mentioned above. The Hamiltonian transformation is originally expressed as

$$
\begin{aligned}
\left\langle \boldsymbol{f}^{\alpha}, \boldsymbol{\mathcal{H}}\boldsymbol{f}^{\beta} \right\rangle &= \left\langle \boldsymbol{f}^{\beta}, \boldsymbol{\mathcal{H}}\boldsymbol{f}^{\alpha} \right\rangle + \sum_{k=1}^{n} \left[u_{x;k}^{\beta}\sigma_{xx;k}^{\alpha} + u_{z;k}^{\beta}\sigma_{xz;k}^{\alpha} + \varphi_{k}^{\beta}D_{x;k}^{\alpha} + \psi_{k}^{\beta}B_{x;k}^{\alpha} - u_{x;k}^{\alpha}\sigma_{xx;k}^{\beta} - u_{z;k}^{\alpha}\sigma_{xz;k}^{\beta} - \varphi_{k}^{\alpha}D_{x;k}^{\beta} - \psi_{k}^{\alpha}B_{x;k}^{\beta} \right]_{x=x_{k-1}}^{x=x_{k}} \\
&= \left\langle \boldsymbol{f}^{\beta}, \boldsymbol{\mathcal{H}}\boldsymbol{f}^{\alpha} \right\rangle + \sum_{k=1}^{n} \left[u_{x;k}^{\beta}\sigma_{xx;k}^{\alpha} + u_{z;k}^{\beta}\sigma_{xz;k}^{\alpha} + \varphi_{k}^{\beta}D_{x;k}^{\alpha} + \psi_{k}^{\beta}B_{x;k}^{\alpha} - u_{x;k}^{\alpha}\sigma_{xx;k}^{\beta} - u_{z;k}^{\alpha}\sigma_{xz;k}^{\beta} - \varphi_{k}^{\alpha}D_{x;k}^{\beta} - \psi_{k}^{\alpha}B_{x;k}^{\beta} \right]_{x=x_{k-1}}^{x=x_{k}} \\
&\triangleq \left\langle \boldsymbol{f}^{\beta}, \boldsymbol{\mathcal{H}}\boldsymbol{f}^{\alpha} \right\rangle + \left[u_{x;n}^{\beta}\sigma_{xx;n}^{\alpha} + u_{z;n}^{\beta}\sigma_{xz;n}^{\alpha} + \varphi_{n}^{\beta}D_{x;n}^{\alpha} + \psi_{n}^{\beta}B_{x;n}^{\alpha} - u_{x;n}^{\alpha}\sigma_{xx;n}^{\beta} - u_{z;n}^{\alpha}\sigma_{xz;n}^{\beta} - \varphi_{n}^{\alpha}D_{x;n}^{\beta} - \psi_{n}^{\alpha}B_{x;n}^{\beta} \right]_{x=x_{n}} \\
&\quad \cancel{- \left[u_{x;1}^{\beta}\sigma_{xx;1}^{\alpha} + u_{z;1}^{\beta}\sigma_{xz;1}^{\alpha} + \varphi_{1}^{\beta}D_{x;1}^{\alpha} + \psi_{1}^{\beta}B_{x;1}^{\alpha} - u_{x;1}^{\alpha}\sigma_{xx;1}^{\beta} - u_{z;1}^{\alpha}\sigma_{xz;1}^{\beta} - \varphi_{1}^{\alpha}D_{x;1}^{\beta} - \psi_{1}^{\alpha}B_{x;1}^{\beta} \right]_{x=x_{0}}}
\end{aligned}
\tag{B.4}
$$

where the symbol "$\triangleq$" represents that the simplifications are conducted according to the continuity conditions. The last term in Eq. (B.4) vanishes due to the free boundary conditions at $x = x_0$. We may let $\left\langle \boldsymbol{f}^{\alpha}, \boldsymbol{\mathcal{H}}\boldsymbol{f}^{\beta} \right\rangle = \left\langle \boldsymbol{f}^{\beta}, \boldsymbol{\mathcal{H}}\boldsymbol{f}^{\alpha} \right\rangle$ to satisfy the boundary conditions at $x = x_n$, which indicates that θ_1 is determined using symplectic orthogonality. To elucidate, we may regard $(x - \theta_1)$ as a shift of the coordinate system toward the positive x-direction by θ_1.

Appendix C. Coefficients for algebraic equations and relations

The parameters in Eq. (36) are:

$$
\begin{aligned}
\Lambda_{0;k} = &\left(\left(a_{10;k}^{2} - a_{9;k}a_{12;k}\right)a_{4;k}^{2} + 2a_{6;k}\left(a_{10;k}a_{11;k} + a_{8;k}a_{12;k}\right)a_{4;k} + a_{6;k}^{2}a_{11;k}^{2} + a_{5;k}a_{9;k}a_{11;k}^{2} + 2a_{5;k}a_{8;k}a_{10;k}a_{11;k} + a_{5;k}a_{8;k}^{2}a_{12;k}\right. \\
&\left. + \left(\left(a_{6;k}^{2} + a_{5;k}a_{9;k}\right)a_{12;k} - a_{5;k}a_{10;k}^{2}\right)a_{13;k} + a_{7;k}^{2}\left(a_{8;k}^{2} + a_{9;k}a_{13;k}\right) + 2a_{7;k}\left(a_{4;k}\left(a_{8;k}a_{10;k} + a_{9;k}a_{11;k}\right) + a_{6;k}\left(a_{10;k}a_{13;k} - a_{8;k}a_{11;k}\right)\right)\right)\left(a_{15;k}^{2} - a_{14;k}a_{16;k}\right)
\end{aligned}
\tag{C.1}
$$

$$
\begin{aligned}
\Lambda_{1;k} =& \Big(a_{12;k}a_{8;k}^2 + 2a_{10;k}a_{11;k}a_{8;k} - a_{10;k}^2a_{13;k} + a_{9;k}\left(a_{11;k}^2 + a_{12;k}a_{13;k}\right)\Big)a_{14;k}a_{2;k}^2 - 2a_{2;k}a_{7;k}a_{8;k}^2a_{14;k} + 2a_{2;k}a_{6;k}a_{8;k}a_{11;k}a_{14;k} + 2a_{2;k}a_{6;k}a_{11;k}^2a_{15;k} \\
&-2a_{7;k}a_{8;k}a_{11;k}a_{15;k}a_{2;k} - 4a_{1;k}a_{8;k}a_{10;k}a_{11;k}a_{15;k}a_{2;k} - 2a_{1;k}\left(a_{9;k}\left(a_{11;k}^2 + a_{12;k}a_{13;k}\right) - a_{10;k}^2a_{13;k}\right)a_{15;k}a_{2;k} + 2a_{4;k}a_{11;k}\left(a_{10;k}a_{15;k} - a_{9;k}a_{14;k}\right)a_{2;k} \\
&+2a_{7;k}a_{13;k}\left(a_{10;k}a_{15;k} - a_{9;k}a_{14;k}\right)a_{2;k} + 2a_{4;k}a_{8;k}\left(a_{12;k}a_{15;k} - a_{10;k}a_{14;k}\right)a_{2;k} + 2a_{6;k}a_{13;k}\left(a_{12;k}a_{15;k} - a_{10;k}a_{14;k}\right)a_{2;k} - 2a_{4;k}a_{10;k}^2a_{15;k}^2 \\
&+a_{3;k}a_{9;k}a_{11;k}^2a_{15;k}^2 - 2a_{7;k}a_{8;k}a_{10;k}a_{15;k}^2 - 2a_{7;k}a_{9;k}a_{11;k}a_{15;k}^2 - 2a_{6;k}a_{10;k}a_{11;k}a_{15;k}^2 + 2a_{3;k}a_{8;k}a_{10;k}a_{11;k}a_{15;k}^2 + a_{3;k}a_{8;k}^2a_{12;k}a_{15;k}^2 - 2a_{6;k}a_{8;k}a_{12;k}a_{15;k}^2 \\
&+2a_{4;k}a_{9;k}a_{12;k}a_{15;k}^2 - a_{3;k}a_{10;k}^2a_{13;k}a_{15;k}^2 + a_{3;k}a_{9;k}a_{12;k}a_{13;k}a_{15;k}^2 - a_{5;k}a_{8;k}^2a_{14;k} - 2a_{4;k}a_{6;k}a_{8;k}a_{14;k} + a_{4;k}^2a_{9;k}a_{14;k} - a_{6;k}^2a_{13;k}a_{14;k} - a_{5;k}a_{9;k}a_{13;k}a_{14;k} \\
&-2a_{4;k}a_{7;k}a_{8;k}a_{15;k} - 2a_{4;k}^2a_{10;k}a_{15;k} + 2a_{1;k}a_{4;k}a_{8;k}a_{10;k}a_{15;k} - 2a_{4;k}a_{6;k}a_{11;k}a_{15;k} - 2a_{5;k}a_{8;k}a_{11;k}a_{15;k} - 2a_{1;k}a_{6;k}a_{8;k}a_{11;k}a_{15;k} + 2a_{1;k}a_{4;k}a_{9;k}a_{11;k}a_{15;k} \\
&+2a_{1;k}a_{8;k}^2\left(a_{7;k} - a_{2;k}a_{12;k}\right)a_{15;k} - 2a_{6;k}a_{7;k}a_{13;k}a_{15;k} + 2a_{1;k}a_{7;k}a_{9;k}a_{13;k}a_{15;k} + 2a_{5;k}a_{10;k}a_{13;k}a_{15;k} + 2a_{1;k}a_{6;k}a_{10;k}a_{13;k}a_{15;k} \\
&+a_{16;k}\Big(\Big(a_{12;k}a_{8;k}^2 + 2a_{10;k}a_{11;k}a_{8;k} - a_{10;k}^2a_{13;k} + a_{9;k}\left(a_{11;k}^2 + a_{12;k}a_{13;k}\right)\Big)a_{1;k}^2 - 2\Big(a_{7;k}\left(a_{10;k}a_{13;k} - a_{8;k}a_{11;k}\right) + a_{6;k}\left(a_{11;k}^2 + a_{12;k}a_{13;k}\right)\Big)a_{1;k} \\
&-a_{5;k}a_{11;k}^2 + a_{4;k}^2a_{12;k} - a_{7;k}^2a_{13;k} - a_{5;k}a_{12;k}a_{13;k} - 2a_{4;k}\Big(a_{7;k}a_{11;k} + a_{1;k}\left(a_{10;k}a_{11;k} + a_{8;k}a_{12;k}\right) + \left(a_{9;k}a_{12;k} - a_{10;k}^2\right)a_{14;k}\Big) \\
&+\Big(2a_{7;k}\left(a_{8;k}a_{10;k} + a_{9;k}a_{11;k}\right) + 2a_{6;k}\left(a_{10;k}a_{11;k} + a_{8;k}a_{12;k}\right) - a_{3;k}\left(a_{12;k}a_{8;k}^2 + 2a_{10;k}a_{11;k}a_{8;k} + a_{9;k}a_{11;k}^2 + \left(a_{9;k}a_{12;k} - a_{10;k}^2\right)a_{13;k}\right)\Big)a_{14;k}\Big)
\end{aligned}
\tag{C.2}
$$

$$
\begin{aligned}
\Lambda_{2;k} =& \left(a_{8;k}^2 + a_{9;k}a_{13;k}\right)a_{1;k}^2 + 2\Big(-a_{6;k}a_{13;k} + a_{2;k}\left(a_{8;k}a_{11;k} - a_{10;k}a_{13;k}\right) - \left(a_{8;k}a_{10;k} + a_{9;k}a_{11;k}\right)a_{15;k} + \left(a_{10;k}a_{11;k} + a_{8;k}a_{12;k}\right)a_{16;k}\Big)a_{1;k} + a_{4;k}^2 \\
&+a_{2;k}^2a_{11;k}^2 + a_{10;k}^2a_{15;k}^2 - a_{9;k}a_{12;k}a_{15;k}^2 - a_{5;k}a_{13;k} - 2a_{2;k}a_{7;k}a_{13;k} + a_{2;k}^2a_{12;k}a_{13;k} + a_{8;k}\left(2a_{6;k} - a_{3k;}a_{8;k}\right)a_{14;k} + 2a_{2;k}a_{8;k}a_{10;k}a_{14;k} \\
&+2a_{2;k}a_{9;k}a_{11;k}a_{14;k} - a_{3;k}a_{9;k}a_{13;k}a_{14;k} + 2a_{7;k}a_{8;k}a_{15;k} + 2a_{6;k}a_{11;k}a_{15;k} - 2a_{3;k}a_{8;k}a_{11;k}a_{15;k} - 2a_{2;k}a_{10;k}a_{11;k}a_{15;k} - 2a_{2;k}a_{8;k}a_{12;k}a_{15;k} + 2a_{3;k}a_{10;k}a_{13;k}a_{15;k} \\
&-\Big(-2a_{7;k}a_{11;k} + a_{3;k}\left(a_{11;k}^2 + a_{12;k}a_{13;k}\right) + \left(a_{10;k}^2 - a_{9;k}a_{12;k}\right)a_{14;k}\Big)a_{16;k} - 2a_{4;k}\left(a_{1;k}a_{8;k} + a_{2;k}a_{11;k} + a_{9;k}a_{14;k} - 2a_{10;k}a_{15;k} + a_{12;k}a_{16;k}\right)
\end{aligned}
\tag{C.3}
$$

$$
\Lambda_{3;k} = -2a_{4;k} + 2a_{1;k}a_{8;k} + 2a_{2;k}a_{11;k} - a_{3;k}a_{13;k} + a_{9;k}a_{14;k} - 2a_{10;k}a_{15;k} + a_{12;k}a_{16;k} \tag{C.4}
$$

The parameters of the roots in Eq. (37) are given by

$$
\begin{aligned}
\chi_{1;k} &= -\varpi_{1;k} - \frac{\Lambda_{1;k}}{4\Lambda_{0;k}} - \frac{1}{2}\sqrt{-\varpi_{2;k} + \varpi_{3;k}}, \quad \chi_{2;k} = -\varpi_{1;k} - \frac{\Lambda_{1;k}}{4\Lambda_{0;k}} + \frac{1}{2}\sqrt{-\varpi_{2;k} + \varpi_{3;k}} \\
\chi_{3;k} &= \varpi_{1;k} - \frac{\Lambda_{1;k}}{4\Lambda_{0;k}} - \frac{1}{2}\sqrt{\varpi_{2;k} + \varpi_{3;k}}, \qquad \chi_{4;k} = \varpi_{1;k} - \frac{\Lambda_{1;k}}{4\Lambda_{0;k}} + \frac{1}{2}\sqrt{\varpi_{2;k} + \varpi_{3;k}}
\end{aligned}
$$

where

$$\varpi_{1;k}=\frac{1}{2}\left(\frac{\sqrt[3]{2\Lambda_{2;k}^3-72\Lambda_{0;k}\Lambda_{2;k}-9\Lambda_{1;k}\Lambda_{3;k}\Lambda_{2;k}+27\Lambda_{1;k}^2+27\Lambda_{0;k}\Lambda_{3;k}^2+\sqrt{\left(2\Lambda_{2;k}^3-72\Lambda_{0;k}\Lambda_{2;k}-9\Lambda_{1;k}\Lambda_{3;k}\Lambda_{2;k}+27\Lambda_{1;k}^2+27\Lambda_{0;k}\Lambda_{3;k}^2\right)^2-4\left(\Lambda_{2;k}^2+12\Lambda_{0;k}-3\Lambda_{1;k}\Lambda_{3;k}\right)^3}}}{3\sqrt[3]{2}\Lambda_{0;k}}+\frac{\Lambda_{1;k}^2}{4\Lambda_{0;k}^2}-\frac{2\Lambda_{2;k}}{3\Lambda_{0;k}}\right.$$

$$\left.+\frac{\sqrt[3]{2}\left(\Lambda_{2;k}^2+12\Lambda_{0;k}-3\Lambda_{1;k}\Lambda_{3;k}\right)}{3\Lambda_{0;k}\sqrt[3]{2\Lambda_{2;k}^3-72\Lambda_{0;k}\Lambda_{2;k}-9\Lambda_{1;k}\Lambda_{3;k}\Lambda_{2;k}+27\Lambda_{1;k}^2+27\Lambda_{0;k}\Lambda_{3;k}^2+\sqrt{\left(2\Lambda_{2;k}^3-72\Lambda_{0;k}\Lambda_{2;k}-9\Lambda_{1;k}\Lambda_{3;k}\Lambda_{2;k}+27\Lambda_{1;k}^2+27\Lambda_{0;k}\Lambda_{3;k}^2\right)^2-4\left(\Lambda_{2;k}^2+12\Lambda_{0;k}-3\Lambda_{1;k}\Lambda_{3;k}\right)^3}}}\right)^{\frac{1}{2}}$$

$$\varpi_{2;k}=\left(-\frac{\Lambda_{1;k}^3}{\Lambda_{0;k}^3}+\frac{4\Lambda_{2;k}\Lambda_{1;k}}{\Lambda_{0;k}^2}-\frac{8\Lambda_{3;k}}{\Lambda_{0;k}}\right)\Bigg/$$

$$\left(4\left(\frac{\sqrt[3]{2\Lambda_{2;k}^3-72\Lambda_{0;k}\Lambda_{2;k}-9\Lambda_{1;k}\Lambda_{3;k}\Lambda_{2;k}+27\Lambda_{1;k}^2+27\Lambda_{0;k}\Lambda_{3;k}^2+\sqrt{\left(2\Lambda_{2;k}^3-72\Lambda_{0;k}\Lambda_{2;k}-9\Lambda_{1;k}\Lambda_{3;k}\Lambda_{2;k}+27\Lambda_{1;k}^2+27\Lambda_{0;k}\Lambda_{3;k}^2\right)^2-4\left(\Lambda_{2;k}^2+12\Lambda_{0;k}-3\Lambda_{1;k}\Lambda_{3;k}\right)^3}}}{3\sqrt[3]{2}\Lambda_{0;k}}\right.\right.$$

$$\left.\left.+\frac{\Lambda_{1;k}^2}{4\Lambda_{0;k}^2}+\frac{\sqrt[3]{2}\left(\Lambda_{2;k}^2+12\Lambda_{0;k}-3\Lambda_{1;k}\Lambda_{3;k}\right)}{3\Lambda_0\sqrt[3]{2\Lambda_2^3-72\Lambda_0\Lambda_2-9\Lambda_1\Lambda_3\Lambda_2+27\Lambda_1^2+27\Lambda_0\Lambda_3^2+\sqrt{\left(2\Lambda_2^3-72\Lambda_0\Lambda_2-9\Lambda_1\Lambda_3\Lambda_2+27\Lambda_1^2+27\Lambda_0\Lambda_3^2\right)^2-4\left(\Lambda_2^2+12\Lambda_0-3\Lambda_1\Lambda_3\right)^3}}}-\frac{2\Lambda_2}{3\Lambda_0}\right)^{\frac{1}{2}}\right)$$

$$\varpi_{3;k}=-\frac{\sqrt[3]{2\Lambda_{2;k}^3-72\Lambda_{0;k}\Lambda_{2;k}-9\Lambda_{1;k}\Lambda_{3;k}\Lambda_{2;k}+27\Lambda_{1;k}^2+27\Lambda_{0;k}\Lambda_{3;k}^2+\sqrt{\left(2\Lambda_{2;k}^3-72\Lambda_{0;k}\Lambda_{2;k}-9\Lambda_{1;k}\Lambda_{3;k}\Lambda_{2;k}+27\Lambda_{1;k}^2+27\Lambda_{0;k}\Lambda_{3;k}^2\right)^2-4\left(\Lambda_{2;k}^2+12\Lambda_{0;k}-3\Lambda_{1;k}\Lambda_{3;k}\right)^3}}}{3\sqrt[3]{2}\Lambda_{0;k}}+\frac{\Lambda_{1;k}^2}{2\Lambda_{0;k}^2}-\frac{4\Lambda_{2;k}}{3\Lambda_{0;k}}$$
$$-\frac{\sqrt[3]{2}\left(\Lambda_{2;k}^2+12\Lambda_{0;k}-3\Lambda_{1;k}\Lambda_{3;k}\right)}{3\Lambda_{0;k}\sqrt[3]{2\Lambda_{2;k}^3-72\Lambda_{0;k}\Lambda_{2;k}-9\Lambda_{1;k}\Lambda_{3;k}\Lambda_{2;k}+27\Lambda_{1;k}^2+27\Lambda_{0;k}\Lambda_{3;k}^2+\sqrt{\left(2\Lambda_{2;k}^3-72\Lambda_{0;k}\Lambda_{2;k}-9\Lambda_{1;k}\Lambda_{3;k}\Lambda_{2;k}+27\Lambda_{1;k}^2+27\Lambda_{0;k}\Lambda_{3;k}^2\right)^2-4\left(\Lambda_{2;k}^2+12\Lambda_{0;k}-3\Lambda_{1;k}\Lambda_{3;k}\right)^3}}}$$

and the properties of the roots can be determined from the coefficients of the quartic equation.

If the roots of Eq. (36) are nonequal and real (i.e., $\eta_{1,2;k}=\pm\sqrt{\chi_{1;k}}\mu$, $\eta_{3,4;k}=\pm\sqrt{\chi_{2;k}}\mu$, $\eta_{5,6;k}=\pm\sqrt{\chi_{3;k}}\mu$, $\eta_{7,8;k}=\pm\sqrt{\chi_{4;k}}\mu$), the general solution set can be rewritten in another form:

$$\{\cosh(\sqrt{\chi_{1;k}}\mu x),\sinh(\sqrt{\chi_{1;k}}\mu x),\cosh(\sqrt{\chi_{2;k}}\mu x),\sinh(\sqrt{\chi_{2;k}}\mu x),\cosh(\sqrt{\chi_{3;k}}\mu x),\sinh(\sqrt{\chi_{3;k}}\mu x),\cosh(\sqrt{\chi_{4;k}}\mu x),\sinh(\sqrt{\chi_{4;k}}\mu x)\} \tag{C.5}$$

If the roots are nonequal and pure imaginary (i.e., $\eta_{1,2;k}=\pm\mathrm{i}\sqrt{\chi_{1;k}}\mu$, $\eta_{3,4;k}=\pm\mathrm{i}\sqrt{\chi_{2;k}}\mu$, $\eta_{5,6;k}=\pm\mathrm{i}\sqrt{\chi_{3;k}}\mu$, $\eta_{7,8;k}=\pm\mathrm{i}\sqrt{\chi_{4;k}}\mu$), the general solution set is:

$$\{\cos(\sqrt{\chi_{1;k}}\mu x),\sin(\sqrt{\chi_{1;k}}\mu x),\cos(\sqrt{\chi_{2;k}}\mu x),\sin(\sqrt{\chi_{2;k}}\mu x),\cos(\sqrt{\chi_{3;k}}\mu x),\sin(\sqrt{\chi_{3;k}}\mu x),\cos(\sqrt{\chi_{4;k}}\mu x),\sin(\sqrt{\chi_{4;k}}\mu x)\} \tag{C.6}$$

If the roots are mixed such that $\eta_{1,2;k}=\pm\sqrt{\chi_{1;k}}\mu$, $\eta_{3,4;k}=\pm\sqrt{\chi_{2;k}}\mu$, $\eta_{5,6;k}=\pm\sqrt{\chi_{3;k}}\mu$, $\eta_{7,8;k}=\pm\mathrm{i}\sqrt{\chi_{4;k}}\mu$, the general solution is

$$\{\cosh(\sqrt{\chi_{1;k}}\mu x),\sinh(\sqrt{\chi_{1;k}}\mu x),\cosh(\sqrt{\chi_{2;k}}\mu x),\sinh(\sqrt{\chi_{2;k}}\mu x),\cosh(\sqrt{\chi_{3;k}}\mu x),\sinh(\sqrt{\chi_{3;k}}\mu x),\cos(\sqrt{\chi_{4;k}}\mu x),\sin(\sqrt{\chi_{4;k}}\mu x)\} \tag{C.7}$$

If the roots are repeated such that $\eta_{1,2;k}=\pm\mathrm{i}\sqrt{\chi_{1;k}}\mu$, $\eta_{3,4;k}=\pm\mathrm{i}\sqrt{\chi_{1;k}}\mu$, $\eta_{5,6;k}=\pm\mathrm{i}\sqrt{\chi_{2;k}}\mu$, $\eta_{7,8;k}=\pm\mathrm{i}\sqrt{\chi_{3;k}}\mu$, the general solution is

$$\{\cos(\sqrt{\chi_{1;k}}\mu x),\sin(\sqrt{\chi_{1;k}}\mu x),x\cos(\sqrt{\chi_{1;k}}\mu x),x\sin(\sqrt{\chi_{1;k}}\mu x),\cos(\sqrt{\chi_{2;k}}\mu x),\sin(\sqrt{\chi_{2;k}}\mu x),\cos(\sqrt{\chi_{3;k}}\mu x),\sin(\sqrt{\chi_{3;k}}\mu x)\} \tag{C.8}$$

The general solutions for other cases can be deduced similarly, which are omitted here for simplicity.

The coefficients for the relations between the constants in Eq. (39) are:

$$\begin{aligned}
&\Upsilon_{1t;k}=\Xi_{1t;k}/\Theta_{1;k}, \quad \Upsilon_{2t;k}=\Xi_{2t;k}/\Theta_{2;k}, \quad \Upsilon_{3t;k}=\Xi_{3t;k}/\Theta_{2;k}\\
&\Upsilon_{4t;k}=\Xi_{4t;k}/\Theta_{2;k}, \quad \Upsilon_{6t;k}=\Xi_{6t;k}/\Theta_{1;k}, \quad \Upsilon_{7t;k}=\Xi_{7t;k}/\Theta_{1;k}\\
&\Upsilon_{5t;k}=-\eta_{t;k}\,/\,\mu
\end{aligned}$$

where

$$\begin{aligned}
\Theta_{1;k}=&\mu\eta_{t;k}\Big(a_{1;k}a_{8;k}\mu^4+\big(-a_{4;k}+a_{2;k}a_{11;k}+a_{9;k}a_{14;k}-2a_{10;k}a_{15;k}+a_{12;k}a_{16k;}\big)\mu^4\eta_{t;k}+\Big(a_{15;k}\Big(\big(a_{6;k}-a_{1;k}a_{9;k}\big)a_{11;k}+\big(a_{10;k}^2-a_{9;k}a_{12;k}\big)a_{15;k}\Big)\\
&+a_{2;k}a_{11;k}\big(a_{9;k}a_{14;k}-a_{10;k}a_{15;k}\big)+\Big(\big(a_{7;k}+a_{1;k}a_{10;k}\big)a_{11;k}+\big(a_{9;k}a_{12;k}-a_{10;k}^2\big)a_{14;k}\Big)a_{16;k}-a_{4;k}\big(a_{9;k}a_{14;k}-2a_{10;k}a_{15;k}+a_{12;k}a_{16;k}\big)\Big)\mu^2\eta_{t;k}^3\\
&+a_{8;k}\big(a_{6;k}a_{14;k}+\big(a_{7;k}-a_{1;k}a_{10;k}\big)a_{15;k}+a_{2;k}\big(a_{10;k}a_{14;k}-a_{12;k}a_{15;k}\big)+a_{1;k}a_{12;k}a_{16;k}\big)\mu^2\eta_{t;k}^2\\
&-\Big(\Big(\big(a_{7;k}a_{9;k}+a_{6;k}a_{10;k}\big)a_{11;k}+a_{4;k}\big(a_{10;k}^2-a_{9;k}a_{12;k}\big)\Big)\big(a_{15;k}^2-a_{14;k}a_{16;k}\big)\eta_{t;k}^5\Big)-a_{8;k}\big(a_{7;k}a_{10;k}+a_{6;k}a_{12;k}\big)\big(a_{15;k}^2-a_{14;k}a_{16;k}\big)\eta_{t;k}^4\Big)+\mu^7
\end{aligned}\tag{C.9}$$

$$\begin{aligned}
\Theta_{2;k}=&\big(-a_{4;k}+a_{2;k}a_{11;k}+a_{9;k}a_{14;k}-2a_{10;k}a_{15;k}+a_{12;k}a_{16;k}\big)\mu^4\eta_{t;k}^2+a_{1;k}a_{8;k}\mu^4\eta_{t;k}+\Big(a_{15;k}\Big(\big(a_{6;k}-a_{1;k}a_{9;k}\big)a_{11;k}+\big(a_{10;k}^2-a_{9;k}a_{12;k}\big)a_{15k;}\Big)\\
&+a_{2;k}a_{11;k}\big(a_{9;k}a_{14;k}-a_{10;k}a_{15;k}\big)+\Big(\big(a_{7;k}+a_{1;k}a_{10;k}\big)a_{11;k}+\big(a_{9;k}a_{12;k}-a_{10;k}^2\big)a_{14;k}\Big)a_{16;k}-a_{4;k}\big(a_{9;k}a_{14;k}-2a_{10;k}a_{15;k}+a_{12;k}a_{16;k}\big)\Big)\mu^2\eta_{t;k}^4\\
&+a_{8;k}\big(a_{6;k}a_{14;k}+\big(a_{7;k}-a_{1;k}a_{10;k}\big)a_{15;k}+a_{2;k}\big(a_{10;k}a_{14;k}-a_{12;k}a_{15;k}\big)+a_{1;k}a_{12;k}a_{16;k}\big)\mu^2\eta_{t;k}^3\\
&-\Big(\Big(\big(a_{7;k}a_{9;k}+a_{6;k}a_{10;k}\big)a_{11;k}+a_{4;k}\big(a_{10;k}^2-a_{9;k}a_{12;k}\big)\Big)\big(a_{15;k}^2-a_{14;k}a_{16;k}\big)\eta_{t;k}^6-a_{8;k}\big(a_{7;k}a_{10;k}+a_{6;k}a_{12;k}\big)\big(a_{15;k}^2-a_{14;k}a_{16;k}\big)\eta_{t;k}^5+\mu^6
\end{aligned}\tag{C.10}$$

$$
\begin{aligned}
\Xi_{1t;k} = &\left(-a_{12;k}a_{2;k}^2 + 2a_{7;k}a_{2;k} + a_{5;k} + a_{1;k}\left(2a_{6;k} - a_{1;k}a_{9;k} + 2a_{2;k}a_{10;k}\right)\right)\mu^4\eta_{t;k}^2 + a_{3;k}\mu^2\left(\left(a_{9;k}a_{14;k} - 2a_{10;k}a_{15;k} + a_{12;k}a_{16;k}\right)\mu^2\eta_{t;k}^2\right.\\
&+\left(a_{10;k}^2 - a_{9;k}a_{12;k}\right)\left(a_{15;k}^2 - a_{14;k}a_{16;k}\right)\eta_{t;k}^4 + \mu^4\Big) + \Big(a_{10;k}^2a_{14;k}a_{2;k}^2 - a_{9;k}a_{12;k}a_{14;k}a_{2;k}^2 + 2a_{7;k}a_{9;k}a_{14;k}a_{2;k} - 2a_{1;k}a_{10;k}^2a_{15;k}a_{2;k}\\
&+2a_{1;k}a_{9;k}a_{12;k}a_{15;k}a_{2;k} - 2a_{7;k}a_{10;k}a_{15;k}a_{2;k} + a_{6;k}^2a_{14;k} + a_{5;k}a_{9;k}a_{14;k} - 2a_{1;k}a_{7;k}a_{9;k}a_{15;k} - 2a_{5;k}a_{10;k}a_{15;k}\\
&+\left(\left(a_{7;k} + a_{1;k}a_{10;k}\right)^2 + \left(a_{5;k} - a_{1;k}^2a_{9;k}\right)a_{12;k}\right)a_{16;k} + 2a_{6;k}\left(\left(a_{7;k} - a_{1;k}a_{10;k}\right)a_{15;k} + a_{2;k}\left(a_{10;k}a_{14;k} - a_{12;k}a_{15;k}\right) + a_{1;k}a_{12;k}a_{16;k}\right)\Big)\mu^2\eta_{t;k}^4\\
&-\left(\left(a_{9;k}a_{7;k}^2 + 2a_{6;k}a_{10;k}a_{7;k} - a_{5;k}a_{10;k}^2 + \left(a_{6;k}^2 + a_{5;k}a_{9;k}\right)a_{12;k}\right)\left(a_{15;k}^2 - a_{14;k}a_{16;k}\right)\eta_{t;k}^6\right)
\end{aligned}
\tag{C.11}
$$

$$
\begin{aligned}
\Xi_{2t;k} = &\,\eta_{t;k}\left(\left(a_{4;k}a_{9;k}a_{1;k}^2 - \left(a_{4;k}\left(a_{6;k} + 2a_{2;k}a_{10;k}\right) + a_{2;k}a_{6;k}a_{11;k} - \left(a_{7;k}a_{9;k} + a_{6;k}a_{10;k}\right)a_{15;k} + \left(a_{7;k}a_{10;k} + a_{6;k}a_{12;k}\right)a_{16;k}\right)a_{1;k} + a_{2;k}^2\left(a_{4;k}a_{12;k} - a_{7;k}a_{11;k}\right)\right.\right.\\
&-a_{6;k}^2a_{14;k} - a_{3;k}a_{4;k}a_{9;k}a_{14;k} - a_{5;k}a_{9;k}a_{14;k} - a_{2;k}\left(a_{4;k}a_{7;k} + a_{5;k}a_{11;k} + \left(a_{7;k}a_{9;k} + a_{6;k}a_{10;k}\right)a_{14;k}\right) - 2a_{6;k}a_{7;k}a_{15;k} + 2a_{3;k}a_{4;k}a_{10;k}a_{15;k} + 2a_{5;k}a_{10;k}a_{15;k}\\
&\left.+a_{3;k}a_{6;k}a_{11;k}a_{15;k} + a_{2;k}\left(a_{7;k}a_{10;k} + a_{6;k}a_{12;k}\right)a_{15;k} - \left(a_{7;k}^2 - a_{3;k}a_{11;k}a_{7;k} + \left(a_{3;k}a_{4;k} + a_{5;k}\right)a_{12;k}\right)a_{16;k}\right)\eta_{t;k}^2\mu^2\\
&-a_{8;k}\left(a_{6;k}a_{1;k}^2 + \left(a_{5;k} + a_{2;k}a_{7;k}\right)a_{1;k} - a_{3;k}\left(a_{6;k}a_{14;k} + a_{7;k}a_{15;k}\right)\right)\eta_{t;k}\mu^2 + \Big(-\Big(\Big(\left(a_{7;k}a_{9;k} + a_{6;k}a_{10;k}\right)a_{11;k} + a_{4;k}\left(a_{10;k}^2 - a_{9;k}a_{12;k}\right)\Big)a_{16;k}a_{1;k}^2\Big)\\
&+\Big(\Big(a_{4;k}\left(a_{7;k}a_{9;k} + a_{6;k}a_{10;k}\right) + \left(a_{6;k}^2 + a_{5;k}a_{9;k}\right)a_{11;k}\Big)a_{15;k} - \Big(\left(a_{5;k}a_{10;k} - a_{6;k}a_{7;k}\right)a_{11;k} + a_{4;k}\left(a_{7;k}a_{10;k} + a_{6;k}a_{12;k}\right)\Big)a_{16;k}\Big)a_{1;k}\\
&-a_{2;k}^2\left(\left(a_{7;k}a_{9;k} + a_{6;k}a_{10;k}\right)a_{11;k} + a_{4;k}\left(a_{10;k}^2 - a_{9;k}a_{12;k}\right)\right)a_{14;k} + \Big(a_{9;k}a_{7;k}^2 + \left(2a_{6;k}a_{10;k} - a_{3;k}a_{9;k}a_{11;k}\right)a_{7;k} - a_{10;k}\left(\left(a_{3;k}a_{4;k} + a_{5;k}\right)a_{10;k} + a_{3;k}a_{6;k}a_{11;k}\right)\\
&+\left(a_{6;k}^2 + \left(a_{3;k}a_{4;k} + a_{5;k}\right)a_{9;k}\right)a_{12;k}\Big)\left(a_{15;k}^2 - a_{14;k}a_{16;k}\right) + a_{2;k}\Big(\Big(\Big(\left(a_{5;k} + 2a_{1;k}a_{6;k}\right)a_{10;k} - a_{7;k}\left(a_{6;k} - 2a_{1;k}a_{9;k}\right)\Big)a_{11;k}\\
&+a_{4;k}\left(a_{10;k}\left(a_{7;k} + 2a_{1;k}a_{10;k}\right) + \left(a_{6;k} - 2a_{1;k}a_{9;k}\right)a_{12;k}\right)\Big)a_{15;k} - \Big(a_{4;k}\left(a_{7;k}a_{9;k} + a_{6;k}a_{10;k}\right) + \left(a_{6;k}^2 + a_{5;k}a_{9;k}\right)a_{11;k}\Big)a_{14;k}\Big)\Big)\eta_t^4\\
&-a_{8;k}\Big(\left(a_{7;k}a_{10;k} + a_{6;k}a_{12;k}\right)a_{16;k}a_{1;k}^2 + \Big(\left(a_{6;k}a_{7;k} - a_{5;k}a_{10;k}\right)a_{15;k} + \left(a_{7;k}^2 + a_{5;k}a_{12;k}\right)a_{16;k}\Big)a_{1;k} + a_{2;k}^2\left(a_{7;k}a_{10;k} + a_{6;k}a_{12;k}\right)a_{14;k}\\
&+a_{2;k}\Big(\Big(a_{5;k}a_{10;k} - a_{6;k}a_{7;k}\Big)a_{14;k} - \Big(a_{7;k}^2 + 2a_{1;k}a_{10;k}a_{7;k} + \left(a_{5;k} + 2a_{1;k}a_{6;k}\right)a_{12;k}\Big)a_{15;k}\Big) + a_{3;k}\left(a_{7;k}a_{10;k} + a_{6;k}a_{12;k}\right)\Big(a_{15;k}^2 - a_{14;k}a_{16;k}\Big)\Big)\eta_{t;k}^3\\
&-\mu^4\left(a_{3;k}a_{4;k} + a_{5;k} + a_{1;k}a_{6;k} + a_{2;k}a_{7;k}\right)\Big)
\end{aligned}
\tag{C.12}
$$

$$
\begin{aligned}
\Xi_{3t;k} &= a_{3;k}a_{8;k}\mu^4 - \left(a_{6;k} - a_{1;k}a_{9;k} + a_{2;k}a_{10;k}\right)\mu^4\eta_{t;k} + \Big(-a_{10;k}a_{11;k}a_{2;k}^2 + \Big(\left(a_{1;k}a_{9;k} - a_{6;k}\right)a_{11;k} + \left(a_{10;k}^2 - a_{9;k}a_{12;k}\right)a_{15;k}\Big)a_{2;k} \\
&\quad + a_{4;k}\left(a_{6;k} - a_{1;k}a_{9;k} + a_{2;k}a_{10;k}\right) + \Big(a_{6;k}a_{10;k} + a_{9;k}\left(a_{7;k} - a_{3;k}a_{11;k}\right)\Big)a_{15;k} - \Big(a_{10;k}\left(a_{7;k} + a_{1;k}a_{10;k} - a_{3;k}a_{11;k}\right) + \left(a_{6;k} - a_{1;k}a_{9;k}\right)a_{12;k}\Big)a_{16;k}\Big)\mu^2\eta_t^3 \\
&\quad + a_{8;k}\left(a_{5;k} + 2a_{2;k}a_{7;k} + a_{1;k}\left(a_{6;k} + a_{2;k}a_{10;k}\right) - a_{3;k}a_{10;k}a_{15;k} + a_{12;k}\left(a_{3;k}a_{16;k} - a_{2;k}^2\right)\right)\mu^2\eta_{t;k}^2 - \Big(\Big(a_{6;k}^2 + a_{2;k}a_{10;k}a_{6;k} + \left(a_{5;k} + a_{2;k}a_{7;k}\right)a_{9;k}\Big)a_{11;k} \\
&\quad + a_{4;k}\Big(a_{10;k}\left(a_{6;k} + a_{2;k}a_{10;k}\right) + a_{9;k}\left(a_{7;k} - a_{2;k}a_{12;k}\right)\Big)\Big)a_{15;k} + \Big(\Big(a_{7;k}\left(a_{1;k}a_{9;k} - a_{6;k}\right) + \left(a_{5;k} + a_{1;k}a_{6;k}\right)a_{10;k}\Big)a_{11;k} \\
&\quad - a_{4;k}\Big(a_{10;k}\left(a_{7;k} + a_{1;k}a_{10;k}\right) + \left(a_{6;k} - a_{1;k}a_{9;k}\right)a_{12;k}\Big)\Big)a_{16;k}\eta_{t;k}^5 + a_{8;k}\Big(\Big(a_{6;k}\left(a_{7;k} - a_{2;k}a_{12;k}\right) - \left(a_{5;k} + a_{2;k}a_{7;k}\right)a_{10;k}\Big)a_{15;k} \\
&\quad + \left(a_{7;k}^2 + a_{1;k}a_{10;k}a_{7;k} + \left(a_{5;k} + a_{1;k}a_{6;k}\right)a_{12;k}\right)a_{16;k}\Big)\eta_{t;k}^4
\end{aligned}
\tag{C.13}
$$

$$
\begin{aligned}
\Xi_{4t;k} &= \eta_{t;k}\Big(\Big(-a_{7;k} - a_{1;k}a_{10;k} + a_{3;k}a_{11;k} + a_{2;k}a_{12;k}\Big)\mu^4 + \Big(-a_{9;k}a_{11;k}a_{1;k}^2 + 2a_{6;k}a_{11;k}a_{1;k} + a_{2;k}a_{10;k}a_{11;k}a_{1;k} + a_{5;k}a_{11;k} + a_{2;k}a_{7;k}a_{11;k} \\
&\quad + a_{4;k}\left(a_{7;k} + a_{1;k}a_{10;k} - a_{2;k}a_{12;k}\right) - a_{2;k}a_{10;k}^2a_{14;k} - a_{7;k}a_{9;k}a_{14;k} - a_{6;k}a_{10;k}a_{14;k} + a_{3;k}a_{9;k}a_{11;k}a_{14;k} + a_{2;k}a_{9;k}a_{12;k}a_{14;k} \\
&\quad + \Big(a_{10;k}\left(a_{7;k} + a_{1;k}a_{10;k} - a_{3;k}a_{11;k}\right) + \left(a_{6;k} - a_{1;k}a_{9;k}\right)a_{12;k}\Big)a_{15;k}\Big)\mu^2\eta_{t;k}^2 - a_{8;k}\left(a_{10;k}a_{1;k}^2 + \left(a_{7;k} - a_{2;k}a_{12;k}\right)a_{1;k} + a_{3;k}\left(a_{12;k}a_{15;k} - a_{10;k}a_{14;k}\right)\right)\mu^2\eta_{t;k} \\
&\quad + \Big(\Big(\Big(a_{6;k}^2 + a_{2;k}a_{10;k}a_{6;k} + \left(a_{5;k} + a_{2;k}a_{7;k}\right)a_{9;k}\Big)a_{11;k} + a_{4;k}\Big(a_{10;k}\left(a_{6;k} + a_{2;k}a_{10;k}\right) + a_{9;k}\left(a_{7;k} - a_{2;k}a_{12;k}\right)\Big)\Big)a_{14;k} \\
&\quad - \Big(\Big(a_{7;k}\left(a_{1;k}a_{9;k} - a_{6;k}\right) + \left(a_{5;k} + a_{1;k}a_{6;k}\right)a_{10;k}\Big)a_{11;k} + a_{4;k}\Big(a_{10;k}\left(a_{7;k} + a_{1;k}a_{10;k}\right) + \left(a_{6;k} - a_{1;k}a_{9;k}\right)a_{12;k}\Big)\Big)a_{15;k}\Big)\eta_{t;k}^4 \\
&\quad - a_{8;k}\Big(\Big(a_{6;k}\left(a_{7;k} - a_{2;k}a_{12;k}\right) - \left(a_{5;k} + a_{2;k}a_{7;k}\right)a_{10;k}\Big)a_{14;k} + \Big(a_{7;k}^2 + a_{1;k}a_{10;k}a_{7;k} + \left(a_{5;k} + a_{1;k}a_{6;k}\right)a_{12;k}\Big)a_{15;k}\Big)\eta_{t;k}^3\Big)
\end{aligned}
\tag{C.14}
$$

$$
\begin{aligned}
\Xi_{6t;k} &= \eta_{t;k}\Big(-a_{1;k}\mu^6 + \Big(-\Big(\left(a_{6;k} + a_{2;k}a_{10;k}\right)a_{14;k}\Big) + \left(-a_{7;k} + a_{3;k}a_{11;k} + a_{2;k}a_{12;k}\right)a_{15;k} + a_{1;k}\left(a_{4;k} - a_{2;k}a_{11;k} + a_{10;k}a_{15;k} - a_{12;k}a_{16;k}\right)\Big)\mu^4\eta_{t;k}^2 \\
&\quad + a_{8;k}\left(a_{3;k}a_{14;k} - a_{1;k}^2\right)\mu^4\eta_{t;k} + \Big(a_{11;k}\Big(\left(a_{7;k} + 2a_{1;k}a_{10;k}\right)a_{15;k} - a_{6;k}a_{14;k}\Big)a_{2;k} - a_{2;k}^2a_{10;k}a_{11;k}a_{14;k} + a_{15;k}\Big(\left(a_{5;k} + a_{1;k}a_{6;k}\right)a_{11;k} \\
&\quad + \Big(a_{10;k}\left(a_{7;k} - a_{3;k}a_{11;k}\right) + a_{6;k}a_{12;k}\Big)a_{15;k}\Big) - \Big(a_{1;k}\left(a_{7;k} + a_{1;k}a_{10;k}\right)a_{11;k} + \left(a_{10;k}\left(a_{7;k} - a_{3;k}a_{11;k}\right) + a_{6;k}a_{12;k}\right)a_{14;k}\Big)a_{16;k} \\
&\quad + a_{4;k}\Big(a_{6;k}a_{14;k} + \left(a_{7;k} - a_{1;k}a_{10;k}\right)a_{15;k} + a_{2;k}\left(a_{10;k}a_{14;k} - a_{12;k}a_{15;k}\right) + a_{1;k}a_{12;k}a_{16;k}\Big)\Big)\mu^2\eta_{t;k}^4 + a_{8;k}\Big(-a_{12;k}a_{14;k}a_{2;k}^2 + 2\Big(a_{7;k}a_{14;k} + a_{1;k}a_{12;k}a_{15;k}\Big)a_{2;k} \\
&\quad + a_{5;k}a_{14;k} - a_{15;k}\left(2a_{1;k}a_{7;k} + a_{3;k}a_{12;k}a_{15;k}\right) + a_{12;k}\left(a_{3;k}a_{14;k} - a_{1;k}^2\right)a_{16;k}\Big)\mu^2\eta_{t;k}^3 - \Big(\Big(a_{5;k}a_{10;k} - a_{6;k}a_{7;k}\Big)a_{11;k} + a_{4;k}\left(a_{7;k}a_{10;k} + a_{6;k}a_{12;k}\right)\Big)\Big(a_{15;k}^2 - a_{14;k}a_{16;k}\Big)\eta_{t;k}^6 \\
&\quad - a_{8;k}\left(a_{7;k}^2 + a_{5;k}a_{12;k}\right)\Big(a_{15;k}^2 - a_{14;k}a_{16;k}\Big)\eta_{t;k}^5\Big)
\end{aligned}
\tag{C.15}
$$

$$
\begin{aligned}
\Xi_{7t;k} = \eta_{t;k}\Big(&-a_{2;k}\mu^6 - \Big(\Big(a_{11;k}a_{2;k}^2 - \Big(a_{4;k} - a_{9;k}a_{14;k} + a_{10;k}a_{15;k}\Big)a_{2;k} + \Big(a_{6;k} - a_{1;k}a_{9;k}\Big)a_{15;k} + \Big(a_{7;k} + a_{1;k}a_{10;k} - a_{3;k}a_{11;k}\Big)a_{16;k}\Big)\mu^4\eta_{t;k}^2\Big)\\
&+a_{8;k}\Big(a_{3;k}a_{15;k} - a_{1;k}a_{2;k}\Big)\mu^4\eta_{t;k} + \Big(\Big(a_{4;k}a_{9;k}a_{14;k} - \Big(a_{4;k}a_{10;k} + 2\Big(a_{6;k} - a_{1;k}a_{9;k}\Big)a_{11;k}\Big)a_{15;k}\Big)a_{2;k} - a_{2;k}^2a_{9;k}a_{11;k}a_{14;k}\\
&+a_{15;k}\Big(a_{4;k}\Big(a_{6;k} - a_{1;k}a_{9;k}\Big) + \Big(a_{6;k}a_{10;k} + a_{9;k}\Big(a_{7;k} - a_{3;k}a_{11;k}\Big)\Big)a_{15;k}\Big) + \Big(a_{4;k}\Big(a_{7;k} + a_{1;k}a_{10;k}\Big) + \Big(-a_{9;k}a_{1;k}^2 + 2a_{6;k}a_{1;k} + a_{5;k}\Big)a_{11;k}\\
&-\Big(a_{6;k}a_{10;k} + a_{9;k}\Big(a_{7;k} - a_{3;k}a_{11;k}\Big)\Big)a_{14;k}\Big)a_{16;k}\Big)\mu^2\eta_{t;k}^4 + a_{8;k}\Big(\Big(\Big(a_{7;k} + 2a_{1;k}a_{10;k}\Big)a_{15;k} - a_{6;k}a_{14;k}\Big)a_{2;k} - a_{2;k}^2a_{10;k}a_{14;k}\\
&+a_{15;k}\Big(a_{5;k} + a_{1;k}a_{6;k} - a_{3;k}a_{10;k}a_{15;k}\Big) - \Big(a_{1;k}\Big(a_{7;k} + a_{1;k}a_{10;k}\Big) - a_{3;k}a_{10;k}a_{14;k}\Big)a_{16;k}\Big)\mu^2\eta_{t;k}^3 - \Big(a_{4;k}\Big(a_{7;k}a_{9;k} + a_{6;k}a_{10;k}\Big)\\
&+\Big(a_{6;k}^2 + a_{5;k}a_{9;k}\Big)a_{11;k}\Big)\Big(a_{15;k}^2 - a_{14;k}a_{16;k}\Big)\eta_{t;k}^6 + a_{8;k}\Big(a_{6;k}a_{7;k} - a_{5;k}a_{10;k}\Big)\Big(a_{15;k}^2 - a_{14;k}a_{16;k}\Big)\eta_{t;k}^5\Big)
\end{aligned}
\tag{C.16}
$$

Appendix D. Parameters, symplectic orthogonal relations, and transfer matrices in the first numerical example

The recurrence relations for β_{1k} and β_{3k} are:

$$
\begin{cases}
\beta_{1(k+1)} = \dfrac{E_k - E_{k+1}}{2}(x_k - \zeta_2)^2 + \beta_{1k}\\
\beta_{3(k+1)} = 2(1+\nu)(x_k - \zeta_2)\left(\dfrac{\beta_{1k}}{E_k} - \dfrac{\beta_{1(k+1)}}{E_{k+1}}\right) + \beta_{3k} \qquad (1 \le k \le n-1)\\
\qquad\quad = 2(1+\nu)(x_k - \zeta_2)\left(\dfrac{1}{E_k} - \dfrac{1}{E_{k+1}}\right)\beta_{1k} - (1+\nu)\dfrac{E_k - E_{k+1}}{E_{k+1}}(x_k - \zeta_2)^3 + \beta_{3k}
\end{cases}
\tag{D.1}
$$

where $\beta_{11} = -\dfrac{E_1}{2}\zeta_2^2$ and $\beta_{31} = 0$. Through the following symplectic orthogonal relations:

$$
\left\langle \boldsymbol{\Phi}_{0,s}^{(1)}, \boldsymbol{\Phi}_{0,a}^{(1)} \right\rangle = \sum_{k=1}^{n}\int_{x_{k-1}}^{x_k} E_k(x - \zeta_2)\mathrm{d}x = \sum_{k=1}^{n}\frac{E_k}{2}(x_k^2 - x_{k-1}^2) - \zeta_2\sum_{k=1}^{n}E_k(x_k - x_{k-1}) = 0 \tag{D.2}
$$

$$\left\langle \boldsymbol{\Phi}_{0,a}^{(3)}, \boldsymbol{\Phi}_{0,s}^{(1)} \right\rangle = \sum_{k=1}^{n} \int_{x_{k-1}}^{x_k} E_k \left\{ \frac{2+\nu}{6}(x-\zeta_2)^3 + \left[\frac{2(1+\nu)}{E_k} - \zeta_3 \right](x-\zeta_2) + \beta_{3k} + \zeta_4 \right\} \mathrm{d}x + \sum_{k=1}^{n} \int_{x_{k-1}}^{x_k} \left[\frac{E_k}{2}(x-\zeta_2)^2 + \beta_{1k} \right](\nu x - \zeta_1)\mathrm{d}x \tag{D.3}$$

$$\left\langle \boldsymbol{\Phi}_{0,a}^{(2)}, \boldsymbol{\Phi}_{0,a}^{(3)} \right\rangle = \sum_{k=1}^{n} \int_{x_{k-1}}^{x_k} E_k (x-\zeta_2) \left\{ \frac{2+\nu}{6}(x-\zeta_2)^3 + \left[\frac{2(1+\nu)}{E_k} - \zeta_3 \right](x-\zeta_2) + \beta_{3k} + \zeta_4 \right\} \mathrm{d}x + \sum_{k=1}^{n} \int_{x_{k-1}}^{x_k} \left[\frac{1}{2}\nu(x-\zeta_2)^2 + \zeta_3 \right] \left[\frac{E_k}{2}(x-\zeta_2)^2 + \beta_{1k} \right] \mathrm{d}x \tag{D.4}$$

we obtain:

$$\zeta_2 = \frac{\sum_{k=1}^{n} \frac{E_k}{2}(x_k^2 - x_{k-1}^2)}{\sum_{k=1}^{n} E_k (x_k - x_{k-1})} \tag{D.5}$$

$$\zeta_4 = -\frac{\sum_{k=1}^{n} E_k \left\{ \frac{2+\nu}{24}\left[(x_k-\zeta_2)^4 - (x_{k-1}-\zeta_2)^4 \right] + \frac{1+\nu}{E_k}\left[(x_k-\zeta_2)^2 - (x_{k-1}-\zeta_2)^2 \right] + \beta_{3k}(x_k - x_{k-1}) \right\}}{\sum_{k=1}^{n} E_k (x_k - x_{k-1})} \tag{D.6}$$

$$\zeta_3 = \frac{\sum_{k=1}^{n} \int_{x_{k-1}}^{x_k} E_k \left\{ \frac{2+\nu}{6}(x-\zeta_2)^4 + \frac{2(1+\nu)}{E_k}(x-\zeta_2)^2 + (\beta_{3k} + \zeta_4)(x-\zeta_2) \right\} \mathrm{d}x + \sum_{k=1}^{n} \int_{x_{k-1}}^{x_k} \frac{1}{2}\nu(x-\zeta_2)^2 \left[\frac{E_k}{2}(x-\zeta_2)^2 + \beta_{1k} \right] \mathrm{d}x}{\sum_{k=1}^{n} \int_{x_{k-1}}^{x_k} \left[\frac{E_k}{2}(x-\zeta_2)^2 - \beta_{1k} \right] \mathrm{d}x} \tag{D.7}$$

$$\zeta_1 = \frac{\sum_{k=1}^{n} \int_{x_{k-1}}^{x_k} \nu x \left[\frac{E_k}{2}(x-\zeta_2)^2 + \beta_{1k} \right] \mathrm{d}x - \sum_{k=1}^{n} \int_{x_{k-1}}^{x_k} E_k \zeta_3 (x-\zeta_2)\mathrm{d}x}{\sum_{k=1}^{n} \int_{x_{k-1}}^{x_k} \left[\frac{E_k}{2}(x-\zeta_2)^2 + \beta_{1k} \right] \mathrm{d}x} \tag{D.8}$$

where ζ_2 is determined, while ζ_1,ζ_3, and ζ_4 are merely constrained by the two symplectic orthogonal relations in Eqs. (D.3) and (D.4), which suggest a practical

approach for deriving solutions. We may therefore conveniently set one parameter and subsequently solve for the others. As evidenced by the symplectic expansion, there is no necessity to explicitly derive the values of ζ_1,ζ_3, and ζ_4.

The constants in Eq. (63) are derived as:

$$\begin{cases} \mathcal{A}_{1n;k} = -\dfrac{(1-\nu)\mathcal{D}_{3n;k} + \mu_n(1+\nu)\mathcal{D}_{1n;k}}{E_k\mu_n^2}, & \mathcal{A}_{2n;k} = \dfrac{(\nu-1)\mathcal{D}_{4n;k} + \mu_n(1+\nu)\mathcal{D}_{2n;k}}{E_k\mu_n^2}, & \mathcal{A}_{3n;k} = \dfrac{\mathcal{D}_{3n;k}(1+\nu)}{E_k\mu_n}, & \mathcal{A}_{4n;k} = -\dfrac{\mathcal{D}_{4n;k}(1+\nu)}{E_k\mu_n} \\ \mathcal{B}_{1n;k} = \dfrac{-2\mathcal{D}_{3n;k} + \mu_n(1+\nu)\mathcal{D}_{1n;k}}{E_k\mu_n^2}, & \mathcal{B}_{2n;k} = \dfrac{2\mathcal{D}_{4n;k} + \mu_n(1+\nu)\mathcal{D}_{2n;k}}{E_k\mu_n^2}, & \mathcal{B}_{3n;k} = \dfrac{\mathcal{D}_{3n;k}(1+\nu)}{E_k\mu_n}, & \mathcal{B}_{4n;k} = \dfrac{\mathcal{D}_{4n;k}(1+\nu)}{E_k\mu_n} \\ \mathcal{C}_{1n;k} = -\dfrac{\mathcal{D}_{3n;k} + \mathcal{D}_{1n;k}\mu_n}{\mu_n}, & \mathcal{C}_{2n;k} = \mathcal{D}_{2n;k} - \dfrac{\mathcal{D}_{4n;k}}{\mu_n}, & \mathcal{C}_{3n;k} = \mathcal{D}_{3n;k}, & \mathcal{C}_{4n;k} = -\mathcal{D}_{4n;k} \end{cases} \tag{D.9}$$

The recurrence relations are deduced in matrix form of:

$$\begin{Bmatrix} \mathcal{D}_{1n;i+1} \\ \mathcal{D}_{2n;i+1} \\ \mathcal{D}_{3n;i+1} \\ \mathcal{D}_{4n;i+1} \end{Bmatrix} = \prod_{k=1}^{i} \left[\boldsymbol{\mathcal{M}}_{n;(k+1)}^{-1} \boldsymbol{\mathcal{M}}_{n;k} \right]_{x=x_k} \begin{Bmatrix} \mathcal{D}_{1n;1} \\ \mathcal{D}_{2n;1} \\ \mathcal{D}_{3n;1} \\ \mathcal{D}_{4n;1} \end{Bmatrix} \tag{D.10}$$

along with the equations for the global state vector:

$$\begin{Bmatrix} u_{z;k} \\ u_{x;k} \\ \sigma_{zz;k} \\ \sigma_{xz;k} \end{Bmatrix} = \left[\boldsymbol{\mathcal{M}}'_{n;k} \right]_x \begin{Bmatrix} \mathcal{D}_{1n;k} \\ \mathcal{D}_{2n;k} \\ \mathcal{D}_{3n;k} \\ \mathcal{D}_{4n;k} \end{Bmatrix} \tag{D.11}$$

where

$$\left[\boldsymbol{\mathcal{M}}_{n;k}\right]_x = \begin{bmatrix} -\dfrac{(1+\nu)\cos(\mu_n x)}{E_k\mu_n} & \dfrac{(1+\nu)\sin(\mu_n x)}{E_k\mu_n} & \dfrac{(\nu-1)\cos(\mu_n x)+\mu_n(1+\nu)x\sin(\mu_n x)}{E_k\mu_n^2} & -\dfrac{(1-\nu)\sin(\mu_n x)+\mu_n(1+\nu)x\cos(\mu_n x)}{E_k\mu_n^2} \\ \dfrac{(1+\nu)\sin(\mu_n x)}{E_k\mu_n} & \dfrac{(1+\nu)\cos(\mu_n x)}{E_k\mu_n} & \dfrac{-2\sin(\mu_n x)+\mu_n(1+\nu)x\cos(\mu_n x)}{E_k\mu_n^2} & \dfrac{2\cos(\mu_n x)+\mu_n(1+\nu)x\sin(\mu_n x)}{E_k\mu_n^2} \\ \sin(\mu_n x) & \cos(\mu_n x) & x\cos(\mu_n x) & x\sin(\mu_n x) \\ \cos(\mu_n x) & -\sin(\mu_n x) & -\dfrac{\cos(\mu_n x)+\mu_n x\sin(\mu_n x)}{\mu_n} & \dfrac{-\sin(\mu_n x)+\mu_n x\cos(\mu_n x)}{\mu_n} \end{bmatrix} \tag{D.12}$$

$$\left[\boldsymbol{\mathcal{M}}'_{n;k}\right]_x = \begin{bmatrix} -\dfrac{(1+\nu)\cos(\mu_n x)}{E_k\mu_n} & \dfrac{(1+\nu)\sin(\mu_n x)}{E_k\mu_n} & \dfrac{(\nu-1)\cos(\mu_n x)+\mu_n(1+\nu)x\sin(\mu_n x)}{E_k\mu_n^2} & -\dfrac{(1-\nu)\sin(\mu_n x)+\mu_n(1+\nu)x\cos(\mu_n x)}{E_k\mu_n^2} \\ \dfrac{(1+\nu)\sin(\mu_n x)}{E_k\mu_n} & \dfrac{(1+\nu)\cos(\mu_n x)}{E_k\mu_n} & \dfrac{-2\sin(\mu_n x)+\mu_n(1+\nu)x\cos(\mu_n x)}{E_k\mu_n^2} & \dfrac{2\cos(\mu_n x)+\mu_n(1+\nu)x\sin(\mu_n x)}{E_k\mu_n^2} \\ -\cos(\mu_n x) & \sin(\mu_n x) & \dfrac{-\cos(\mu_n x)+\mu_n x\sin(\mu_n x)}{\mu_n} & -\dfrac{\sin(\mu_n x)+\mu_n x\cos(\mu_n x)}{\mu_n} \\ \sin(\mu_n x) & \cos(\mu_n x) & x\cos(\mu_n x) & x\sin(\mu_n x) \end{bmatrix} \tag{D.13}$$

In addition, the governing equations for the generalized plane-strain model of the k-th layer is:

$$\frac{\partial}{\partial z}\begin{Bmatrix} u_{z;k} \\ u_{y;k} \\ u_{x;k} \\ \sigma_{zz;k} \\ \sigma_{zy;k} \\ \sigma_{zx;k} \end{Bmatrix} = \left[\begin{array}{ccc:ccc} 0 & 0 & -\frac{\nu}{1-\nu}\frac{\partial}{\partial x} & \frac{(1+\nu)(1-2\nu)}{E_k(1-\nu)} & 0 & 0 \\ 0 & 0 & 0 & 0 & \frac{2(1+\nu)}{E_k} & 0 \\ -\frac{\partial}{\partial x} & 0 & 0 & 0 & 0 & \frac{2(1+\nu)}{E_k} \\ \hdashline 0 & 0 & 0 & 0 & 0 & -\frac{\partial}{\partial x} \\ 0 & -\frac{E_k}{2(1+\nu)}\frac{\partial^2}{\partial x^2} & 0 & 0 & 0 & 0 \\ 0 & 0 & -\frac{E_k}{1-\nu^2}\frac{\partial^2}{\partial x^2} & -\frac{\nu}{1-\nu}\frac{\partial}{\partial x} & 0 & 0 \end{array}\right] \begin{Bmatrix} u_{z;k} \\ u_{y;k} \\ u_{x;k} \\ \sigma_{zz;k} \\ \sigma_{zy;k} \\ \sigma_{zx;k} \end{Bmatrix} \tag{D.14}$$

The corresponding supplementary equations are:

$$\begin{cases} \sigma_{xx;k} = \dfrac{E_k}{1-\nu^2}\dfrac{\partial u_{x;k}}{\partial x} + \dfrac{\nu}{1-\nu}\sigma_{zz;k} \\ \sigma_{yy;k} = \dfrac{E_k\nu}{1-\nu^2}\dfrac{\partial u_{x;k}}{\partial x} + \dfrac{\nu}{1-\nu}\sigma_{zz;k} \\ \sigma_{xy;k} = \dfrac{E_k}{2(1+\nu)}\dfrac{\partial u_{y;k}}{\partial x} \end{cases} \tag{D.15}$$

References

Chen, L.Z.C., Chen, W.Q, 2024. Symplectic contact analysis of a finite-sized horizontally graded magneto-electro-elastic plane. *Proceedings of the Royal Society A*. https://doi.org/10.1098/rspa.2024.0591.

COMSOL Multiphysics® v. 6.0, 2021. cn.comsol.com. COMSOL AB, Stockholm, Sweden.

Giannakopoulos, A.E., Suresh, S., 1997a. Indentation of solids with gradients in elastic properties: Part I. Point force. *International Journal of Solids and Structures* 34, 2357–2392. https://doi.org/10.1016/S0020-7683(96)00171-0

Giannakopoulos, A.E., Suresh, S., 1997b. Indentation of solids with gradients in elastic properties: Part II. axisymmetric indentors. *International Journal of Solids and Structures* 34, 2393–2428. https://doi.org/10.1016/S0020-7683(96)00172-2

Hertz, H., 1881. Über die Berührung fester elastischer Körper. *J reine und angewandte Mathematik* 92, 156–171.

Itou, S., Shima, Y., 1999. Stress intensity factors around a cylindrical crack in an interfacial zone in composite materials. *International Journal of Solids and Structures* 36, 697–709. https://doi.org/10.1016/S0020-7683(98)00041-9

Jagadeesh, P., Rangappa, S.M., Siengchin, S., 2024. Advanced characterization techniques for nanostructured materials in biomedical applications. *Advanced Industrial and Engineering Polymer Research* 7, 122–143. https://doi.org/10.1016/j.aiepr.2023.03.002

Ke, L.-L., Wang, Y.-S., 2006. Two-dimensional contact mechanics of functionally graded materials with arbitrary spatial variations of material properties. *International Journal of Solids and Structures* 43, 5779–5798. https://doi.org/10.1016/j.ijsolstr.2005.06.081

Ke, L.-L., Wang, Y.-S., 2007. Two-dimensional sliding frictional contact of functionally graded materials. *European Journal of Mechanics - A/Solids* 26, 171–188. https://doi.org/10.1016/j.euromechsol.2006.05.007

Leung, A.Y.T., Zheng, J., 2007. Closed form stress distribution in 2D elasticity for all boundary conditions. *Applied Mathematics and Mechanics-English Editon* 28, 1629–1642. https://doi.org/10.1007/s10483-007-1210-z

Lu, Z.C., Ma, D., Liu, X.J., Lu, Z.P., 2024. High-throughput and data-driven machine learning techniques for discovering high-entropy alloys. *Communications Materials* 5, 76. https://doi.org/10.1038/s43246-024-00487-3

Robertson, I.M., Schuh, C.A., Vetrano, J.S., Browning, N.D., Field, D.P., Jensen, D.J., Miller, M.K., Baker, I., Dunand, D.C., Dunin-Borkowski, R., Kabius, B., Kelly, T., Lozano-Perez, S., Misra, A., Rohrer, G.S., Rollett, A.D., Taheri, M.L., Thompson, G.B., Uchic, M., Wang, X.-L., Was, G., 2011. Towards an integrated materials characterization toolbox. *Journal of Materials Research* 26, 1341–1383. https://doi.org/10.1557/jmr.2011.41

Shen, Y.-L., 2010. *Constrained Deformation of Materials: Devices, Heterogeneous Structures and Thermo-Mechanical Modeling.* Springer US, Boston, MA. https://doi.org/10.1007/978-1-4419-6312-3

Stan, G., King, S.W., 2020. Atomic force microscopy for nanoscale mechanical property characterization. *Journal of Vacuum Science & Technology B, Nanotechnology and Microelectronics: Materials, Processing, Measurement, and Phenomena* 38, 060801. https://doi.org/10.1116/6.0000544

Swaddiwudhipong, S., Tho, K.K., Liu, Z.S., Zeng, K., 2005. Material characterization based on dual indenters. *International Journal of Solids and Structures* 42, 69–83. https://doi.org/10.1016/j.ijsolstr.2004.07.027

Uchida, M., Hirano, I., Nakayama, S., Kaneko, Y., 2024. Direct modeling of non-uniform strain field of heterogeneous materials. *International Journal of Mechanical Sciences* 273, 109225. https://doi.org/10.1016/j.ijmecsci.2024.109225

Wodo, O., Zola, J., Sarath Pokuri, B.S., Du, P., Ganapathysubramanian, B., 2015. Automated, high throughput exploration of process–structure–property relationships using the MapReduce paradigm. *Materials Discovery* 1, 21–28. https://doi.org/10.1016/j.md.2015.12.001

Wu, S.C., Wu, Z.K., Kang, G.Z., Chen, W.Q., Li, J.Y., Ke, L.L., Wang, T.M., Xiao, T.Q., Yuan, Q.X., Hu, C.M., 2021. Research Progress on Multi-dimensional and Multi-scale High-throughput Characterization for Advanced Materials. *Journal of Mechanical Engineering* 57, 37. https://doi.org/10.3901/JME.2021.16.037 (in Chinese)

Xu, D., Zhang, Q., Huo, X., Wang, Y., Yang, M., 2023. Advances in data - assisted high - throughput computations for material design. *Materials Genome Engineering Advances* 1, e11. https://doi.org/10.1002/mgea.11

Yao, W., Zhong, W., Lim, C.W., 2009. *Symplectic elasticity*. World Scientific, New Jersey.

Zhong, W.-X., 1995. *A new systematic methodology for theory of elasticity*. Dalian University of Technology Press, Dalian. (in Chinese)